

# Reliability Evaluation of Individual Predictions: A Data-centric Approach

Nima Shahbazi · Abolfazl Asudeh

Received: date / Accepted: date

**Abstract** At the same time that artificial intelligence (AI) and machine learning are becoming central to human life, their potential harms become more vivid. In the presence of such drawbacks, a critical question to address before using individual predictions for critical decision-making is whether those are reliable.

Aligned with recent efforts on data-centric AI, this paper proposes a novel approach, complementary to the existing work on trustworthy AI, to address the reliability question through the lens of data. Specifically, it associates data sets with distrust quantification that specifies their scope of use for individual predictions. It develops novel algorithms for efficient and effective computation of distrust values. The proposed algorithms learn the necessary components of the measures from the data itself and are sublinear, which makes them scalable to very large and multi-dimensional settings. Furthermore, an estimator is designed to enable no-data access during the query time. Besides theoretical analyses, the algorithms are evaluated experimentally, using multiple real and synthetic data sets and different tasks. The experiment results reflect a consistent correlation between distrust values and model performance. This highlights the necessity of dismissing prediction outcomes for cases with high distrust values, at least for critical decisions.

## 1 Introduction

**Motivation:** Increasingly, data is being used for building predictive models to assist decision making, not only efficiently and at scale but also wisely, accurately, and just. However, AI depends on data, and any data-driven algorithm is “*only as good as the data it works with*” [12]. As a result, “despite their huge promise, AI systems can be brittle and unfair” [83]. Unfortunately, examples of such failures are abundant. Bias in recidivism prediction scores [29, 24], in police decisions [32], in granting loans [28], in job screening [22], and in online advertising [79] are only a few examples illustrating the wide scope of the issue.

In the presence of such failures, any decision-maker using a data-driven predictive model faces a critical question: *should they trust an individual prediction of the model for decision-making?* To further motivate this, let us use the following example:

*Example 1* Consider a judge who needs to decide whether to accept or deny a bail request. Using data-driven predictive models is prevalent in such cases for predicting recidivism [24]. Indeed, such models can be beneficial to help the judge make wise decisions. Suppose the model predicts the queried individual as high risk (or low risk). The judge is aware and concerned about the critics surrounding such models. A major question the judge faces is whether or not they should rely on the prediction outcome to take action for this case. Furthermore, if, for instance, they decide to ignore the model outcome, and hence they need to provide a statement supporting their action, what evidence can they provide?

**Novelty:** In line with the recent trend on data-centric AI [60], in this paper we propose a novel approach, com-

---

N. Shahbazi  
University of Illinois Chicago  
E-mail: nshahb3@uic.edu

A. Asudeh  
University of Illinois Chicago  
E-mail: asudeh@uic.edu

plementary to the existing work on trustworthy AI [83, 42, 52, 74, 58], to address the aforementioned trust question through the lens of *data*. In particular, unlike existing works that generate proper trust information for a given *model*, we associate *data sets* with distrust measures that specify their *scope-of-use for predicting individual cases*. Besides, we note that the bulk of work on trustworthy AI provides information that *supports* the outcome of an ML model. For example, existing work on explainable AI, including [36, 67, 33], aims to find simple explanations and rules that justify the outcome of a model. Conversely, motivated by Example 1, we aim to *raise warning signals* when the outcome of a model is *not* trustworthy. That is, to *cast doubt* when an individual prediction is not reliable.

**Technical Highlights:** We introduce two probabilistic measures *Strong Distrust Measure (SDT)* and *Weak Distrust Measure (WDT)* that specify the reliability of a data set for individual predictions. The distrust measures are defined based on two components:

- *Representativeness*: Predictive models provide only probabilistic guarantees on the average loss over the distribution represented by the data set used for training them. As a result, their predictions are not distribution generalizable [47]. Consequently, if the query point is *not represented* by the data, the guarantees may not hold, hence one cannot rely on the prediction outcome.
- *Uncertainty*: when the query point belongs to an *uncertain* neighborhood where data set tuples have different target values, the model prediction may not be reliable.

The distrust measures can be embedded as widgets in data set profiles [2], nutritional labels [78, 75], and data sheets [31].

**Example 1 (part 2):** Distrust measures raise warning when the fitness of the data set used for drawing a prediction is questionable, helping the judge to be cautious when taking action. Besides, these measures provide quantitative justification to support the judge’s action when they decide to ignore a prediction outcome that is not trustworthy. Suppose the WDT for the query point is low. Besides the score, our system specifies that, for example, lack of representation is the issue, reflected by the low representation score. The judge can then argue to ignore a model outcome for this case, justifying that the model has been built using a data set that misses to represent the given case. □

While being agnostic to the choice of the uncertainty and lack of representation components, we propose an implementation based on the  $k$ -vicinity of a query point. In particular, given the radius of the  $k$ -

vicinity and its uncertainty, we develop functions that return probabilities indicating the lack of representation and uncertainty. We propose methods to *learn* the probabilities *from the data set itself*. We devise proper indexing and algorithms that enable sublinear query processing that *scales* to large data sets.

**Positioning in the context of existing work:** Our work differs from existing literature including model-centric uncertainty quantification, local interpretation techniques, and data coverage in several radical ways:

- We offer a *data-centric* distrust measure, a quantitative reliability warning that measures whether a query point is in the scope of use of a data. Unlike model-centric uncertainty quantification techniques, our techniques reveal a property of the data set that regardless of the constructed model this property stands still.
- Although model-centric techniques such as [43, 64, 20] guarantee a user-specified assurance level of error, this error is still computed over the entire data and consequently *may fail to focus the error on local regions* in data, representing, for example, minority populations in social applications. On the other hand, the local fidelity of our techniques satisfies equal treatment for every query point.
- While some model-centric uncertainty quantification techniques [43, 64] claim considering lack of representation as a source of uncertainty, as we observed in our experiments, they fail to capture the associated uncertainty for such query points in sparse regions. This failure originates from the perfect sampling assumption in development and production data which may not hold in practice. Our measures however properly capture such cases and directly target the lack of representation of a query point.
- The literature on data coverage [10, 11, 50] only focuses on representation, and hence fails to capture uncertainty. Additionally, they only return a binary signal of whether to trust the outcome of the model for a query point or not which practically is not very informative. Whereas our proposed measures target both sources of uncertainty and representation and return a quantitative probabilistic value that is easily interpretable.
- Unlike techniques in interpretable machine learning [56] *justify* (advocate) individual predictions, our technique questions those that it finds unreliable.

**Summary of contributions:** In summary, our contributions in this paper include the following:

1. We propose data set distrust measures to raise warnings when the fitness of a data set for an individual

prediction is questionable. To the best of our knowledge, we are the first to propose data-centric distrust measures, a property associated with data sets.

2. Our proposal is a probabilistic measure based on two components: the query’s lack of representation and uncertainty in the data set. The proposed measures can be extended to different data types and are independent from the model and prediction task (classification and regression). The measures are also agnostic to the choice of metric or approach for computing the two components. Proposing quantitative probabilistic outcomes, our measures are interpretable for the users since beyond the scores, the uncertainty and lack of representation components provide an explanation to justify them.
3. We propose novel algorithms based on the  $k$ -vicinity of a query point to compute the query’s lack of representation and uncertainty. In particular, we “learn” the measurements from the data set itself. We also propose proper preprocessing and algorithms that enable sub-linear query answering that scales to very large and high-dimensional data sets. Furthermore, to enable no-data access during the query time, we build regression models to accurately estimate parameters needed to compute distrust measures. We design an exponential search strategy for constructing large-enough samples for training the estimators.
4. We conduct comprehensive experiments on multiple synthetic and real-world data sets with various scales and dimensions, on different prediction tasks (regression and binary/multi-class classification including text classification and image processing), using several models (such as Logistic Regression, DNN, Random Forest, etc.), and distance measures to (i) validate the effectiveness and consistency of the distrust measures, (ii) evaluate the efficiency and scalability of our algorithms and (iii) evaluate the existing works.

Our extensive proof-of-concept experiments verify a consistent correlation between distrust values and ML performance metrics on a variety of tasks, data sets, and ML algorithms. For tuples that have higher distrust values (meaning they are less reliable w.r.t. to our measures), an ML model is more likely to fail to capture the truth and make a correct decision.

**How to use?** As demonstrated in our experiments, when distrust values for a query point are high, one should discard or at least not rely on the individual prediction for critical decisions. We would like to reiterate that our proposal in this paper is complementary to the existing literature and should be used alongside other techniques and potential approaches for trustworthy AI.

## 2 Related Work

Responsible data science has become a timely topic, to which the data management community has extensively contributed [69, 68, 8, 46, 59, 76, 71, 82, 9, 89, 90]. In particular [27] introduces a data profiling primitive *conformance constraint* to characterize whether inference over a tuple is untrustworthy. By the assumption that the *conformance constraints* always hold, they claim that they can use a tuple’s deviation from the constraint as a proxy to whether trust a model’s outcome for that tuple. Besides, extensive studies on different dimensions of trust in ML and AI have been presented in [42, 52]. It is also worth mentioning the body of work on the notion of trustworthiness of data sources that focuses on the correctness and legitimacy of data sources [38, 23], however despite the similar terminology, it is a different concept from our problem.

Related work also includes [13, 62, 91, 1] that aim to estimate and quantify uncertainty in AI models, however, they have a different perspective on the issue as they extract the uncertainty from models, while our measures are data-centric. Probabilistic classifiers predict a probability distribution over the set of classes for a given query point instead of simply returning the most likely class [87, 88, 65, 61]. A given probability metric such as log loss or Brier score is calculated for each example to evaluate the predicted probabilities. Not all of the common classifiers are intrinsically probabilistic and some return distorted probabilities that need to be calibrated. Prediction probabilities are computed using the model trained for global performance and may not be accurate for the unrepresented regions. Prediction Intervals (PIs) are a common practice for quantifying the uncertainty associated with a model’s prediction of a query point in regression tasks [20, 64, 43]. PIs consist of a lower and upper bound that contains a future observation with a specified level of confidence. Although PIs can be constructed in multiple ways, there is a negative correlation between the quality of the PI and the computational load associated with it [44]. Conformal Prediction (CP) is another standard way of quantifying uncertainty in both classification and regression problems returning confidence intervals and confidence sets respectively, guaranteeing a user-specified confidence level. Benefiting from a heuristic notion of uncertainty in the model of choice, a scoring function  $s(x, y)$  is defined that assigns uncertainty values to query point  $x$  given target variable  $y$  with larger values to the cases that  $x$  and  $y$  disagree more. Next, the  $1 - \alpha$  quantile ( $\alpha$  being the user-specified confidence level) of the calibration set scores is calculated and is used to form the prediction set for the new examples.

line of work	target	fidelity	output	task	components	model advocacy	data profiler
distrust measures (this work)	data	local	probabilistic score	classification regression	lack of certainty lack of representation	challenge	yes
prediction probabilities [87, 88, 65, 61]	model	global	probalistic score	classification	lack of certainty	challenge	no
prediction intervals [43, 64, 20]	model	global	interval	regression	lack of certainty	challenge	no
conformal prediction [7, 70]	model	global	interval set	classification regression	lack of certainty	challenge	no
data coverage [10, 11, 50]	data	local	binary signal	classification regression	lack of representation	challenge	yes
local interpretation [53, 67]	model	local	prediction probability feature effect	classification regression	n/a	support	no
out-of-distribution generalizability [18]	model	global	continuous score	classification regression	lack of representation	challenge	yes

**Fig. 1:** Descriptive comparison of distrust measures and related work

It is important to note that all aforementioned model-centric approaches, including PI and CP, estimate intervals, probabilities, and scores using model(s) built by maximizing the *expected performance on random* sample from the underlying distribution. As a result, while they may provide accurate estimations for the dense regions of data (e.g. majority groups), their estimation accuracy is questionable for the poorly represented regions (e.g. minority groups). In particular, [7] recognizes the lack of guarantees in the performance of CP for such regions. On the contrary, prediction outcomes are specifically unreliable for regions that are unlikely to be sampled. As a result, as we further discuss in § 4.1, such approaches fail for cases that are not represented by the training data. This is consistent with our experimental evaluations. PI and CP methods usually rely on techniques such as bootstrapping and constructing ensembles to elicit uncertainty, which regardless of the number of subsamples or ensembles created, fails to account for the regions that are not represented. Contrarily, our proposed measures are computed *locally* around the query point (in form of lack of certainty and lack of representation) and therefore are equally accurate for different regions of data. Finally, while PI and CP return an interval or set for each query point, the results may be too generic (e.g. including a large set) or lack a proper explanation for the user to make an informed decision.

The notion of data *coverage* is a related topic that has been studied across different settings [39, 10, 50, 11, 80, 3, 57, 4]. For categorical data, uncovered regions are identified in form of value combinations (e.g. Hispanic Females) called patterns. A pattern is uncovered if there are not enough samples matching it [39, 10, 50]. *Coverage* on continuous space is studied in [11]. Accordingly, lack of *coverage* is identified as any point in the data space that doesn't have enough points in a fixed-radius neighborhood around it. Although coverage does not provide a score for an arbitrary query point, following

the idea of whether the point is covered or not, users can decide whether to trust the outcome of the model for that query point.

Out-of-distribution generalizability is another related topic from the ML community that quantifies the degree to which a query point is an outlier in the underlying distribution. Specifically, [18] proposes five metrics for identifying well-represented examples. These metrics are shown to be highly correlated, stable, and model-agnostic. The metrics rank examples based on different measures within ensembles, distance to the decision boundary, or prediction difference of two models for the same query point (holdout retraining). It is important to note that these techniques are model-agnostic in the sense that they have consistent results for different models and parameters, however, unlike our techniques that merely assess representation from the data, they still measure representation within model properties.

Another related topic is the body of work on local interpretation methods for explaining individual predictions [56]. LIME provides local explanations for a model's prediction behavior on query points by substituting the original complex model with a locally interpretable surrogate model. Being a model-agnostic technique, to realize what parts of the input are involved in the prediction, LIME perturbs the query point by creating samples around its neighborhood and observes how the model performs for the perturbed samples. Next, the samples are weighted with regard to their proximity to the original query point, and an interpretable model is constructed on the new samples. The learned model should be locally a good approximation and is used to interpret the original model. We note that interpretation methods justify a model's reasoning for a particular behavior. Conversely, our measures raise warnings to cast doubt when the prediction outcome is not reliable for a specific case.

Figure 1, presents an extensive comparison between the related body of work and our proposed measures



and demonstrates how our measures stand out in the skyline. The techniques are examined based on the following properties:

- *target* specifies whether the technique targets data or model.
- *fidelity* specifies whether the technique evaluates trust locally or only provides global assurance (may fail for sparse regions in the data).
- *output* specifies the outcome of the technique.
- *task* specifies the learning problem.
- *component* specifies the considered complications causing the trust problems.
- *model advocacy* specifies whether the technique questions the outcome of the model or tries to justify it.
- *data profiler* specifies whether or not the outcome of the technique is considered as a property of the data.

To the best of our knowledge, our paper is the first to provide data-centric distrust measures to identify the scope of use of data sets for predicting future query points.

The techniques proposed in this paper rely on the extensive research and advanced algorithms for outlier detection [66, 37, 85, 16] and uncertainty computing [72, 15, 17, 30].

### 3 Preliminaries

#### 3.1 Data Model

Consider a data set  $\mathcal{D}$  with  $n$  tuples, each consisting of  $d$  (observation) attributes  $\mathbf{x} = \langle x_1, x_2, \dots, x_d \rangle$  and a target attribute  $y$ , also known as label attribute<sup>1</sup>. The observation attributes  $\mathbf{x}$  are called the *input space* and the target attribute is called the *output space*. We assume the data set is used for training a prediction model  $h$ , as we shall further explain in § 3.2. Prediction models assume that  $\mathcal{D}$  is a set of iid (independent and identically distributed random) samples<sup>2</sup>, drawn from an (unknown) underlying distribution  $\xi$ . Attribute values may be discrete ordinal, continuous-valued, or non-ordinal categorical. Throughout the paper, we assume ordinal attributes are normalized in the range  $[0, 1]$ , with values drawn from the set of rational or real numbers. For

<sup>1</sup> The measures and the algorithms proposed in this paper extend for data sets with multiple target attributes. In such cases, each measure is defined per each target attribute.

<sup>2</sup> We would like to note that our proposal does not make the iid assumption, which can be violated in practice, especially in presence of issues such as sampling bias. We raise a warning when the data set is not fit to draw a specific prediction. As a result, in such cases, the warnings will be raised more frequently for the query points that are not represented by data.

non-ordinal attributes, we assume one-hot encoding is considered. We use  $\mathbf{t}^j$  to refer to the  $j$ -th tuple in the data set  $\mathcal{D}$  and its values of the observation attributes in particular. Similarly, we use  $y^j$  to refer to the value of the target attribute of  $\mathbf{t}^j$ . For every tuple  $\mathbf{t} \in \mathcal{D}$ , we use the notation  $t_i$  to show the value of  $\mathbf{t}$  on attribute  $x_i \in \mathbf{x}$ .

#### 3.2 Query and Prediction Model

The goal of prediction is to guess the target value  $y$  of a query point based on the observations on  $\mathbf{x}$ . In other words, given a point  $\mathbf{q} = \langle q_1, q_2, \dots, q_d \rangle$ , the goal is to predict the value of the target attribute of  $\mathbf{q}$ . We consider the prediction model  $h : \mathbb{R}^d \rightarrow \mathbb{R}$  as a function that predicts the target value of  $\mathbf{q}$  as  $h(\mathbf{q})$ . When  $y$  is categorical, the task is classification, while regression is considered when  $y$  is continuous.

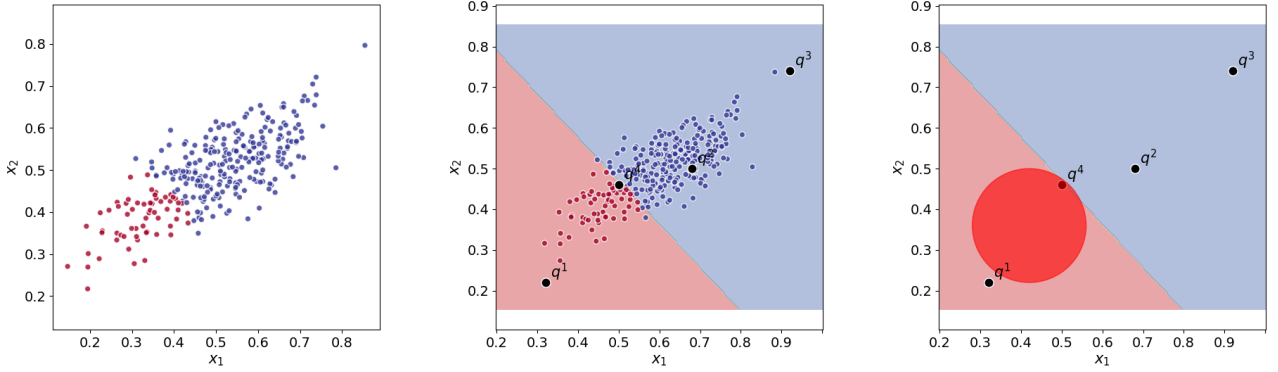
The underlying assumption is that  $\mathbf{q}$  is drawn from the same distribution  $\xi$  from which  $\mathcal{D}$  has been generated. Now, consider the Cartesian product of the input and output space  $\mathbf{x} \times y$ , and fix the hypothesis universe  $\mathcal{H}$  of prediction functions. A learning algorithm  $A$  takes as input the set of samples in the data set  $\mathcal{D}$  and finds a specific function  $h = A(\mathcal{D})$  by minimizing the empirical risk (maximizing the empirical accuracy or minimizing empirical loss) over  $\mathcal{D}$ . Empirical accuracy for classification is computed as the sum of samples in  $\mathcal{D}$  for which the true label is the same as the predicted label. That is,

$$\max \sum_{j=1}^n \mathbb{1}(y^j == h(\mathbf{t}^j)) \quad (1)$$

The equivalent objective for regression is to minimize the empirical error between the target variable and predicted values. Sum of Squares Error (SSE) is the de-facto error measure for regression:

$$\min \sum_{j=1}^n (y^j - h(\mathbf{t}^j))^2 \quad (2)$$

Having a prediction model  $h$  trained by maximizing its empirical accuracy over the sample points in  $\mathcal{D}$ , the model is then used to predict the value of *unseen* target attribute of each query point  $\mathbf{q}$ , observed *after* model deployment, as  $h(\mathbf{q})$ . A central question at this point is whether a decision-maker should rely on the model prediction (at least for critical decisions). In the next section, we propose data-centric measures generated to answer this concern.



(a) The data set  $\mathcal{D}$  generated using a Gaussian distribution where  $x_1$  and  $x_2$  are positively correlated (b) The decision boundary of learned model  $h$  and query points  $\mathbf{q}^1$  to  $\mathbf{q}^4$  (c) Ground-truth boundary, overlaid on the model decision boundary and query points

**Fig. 2:** A toy example (Example 2) representing a binary classification task.

#### 4 Distrust Measures

Not every data set is fit for all data science tasks [78, 10]. An essential requirement for a learning algorithm is that its training data  $\mathcal{D}$  should represent the underlying distribution  $\xi$ . Even if so, the trained model guarantees to perform well only *on average* over the query points drawn from  $\xi$ , not necessarily on a specific query point. To further explain this, let us remind some background from the machine learning theory.

Let  $\mathcal{L}$  be the loss function used by the learning algorithm. Considering the underlying distribution  $\xi$ , the optimal model  $h^* \in \mathcal{H}$  is the one with the minimum expected loss for a random sample drawn from  $\xi$ :

$$\mathcal{E}_{\mathcal{H}}^* = \inf_{h \in \mathcal{H}} \mathbb{E}[\mathcal{L}(h(\mathbf{x}), y)] = \inf_{h \in \mathcal{H}} \int_{\mathbf{x}} \mathcal{L}(h(\mathbf{x}), y) d_{\xi}(\mathbf{x}) \quad (3)$$

Let  $h_n$  be the model generated with the algorithm  $A$  over a data set  $\mathcal{D}$  with  $n$  samples drawn from  $\xi$ . Given the values  $\epsilon, \delta > 0$ , the *sample complexity* [81] of  $A$  is the minimum value of  $n$  such that

$$\mathbb{P}_{\xi}(\mathcal{E}(h_n) - \mathcal{E}^* > \epsilon) \leq \delta \quad (4)$$

If the sample complexity of  $A$  for given values of  $\epsilon$  and  $\delta$  is unbounded, the function space is *not learnable*. The interesting immediate question is whether a distribution-free function is learnable. In other words, is there a learning algorithm  $A$  such that its sample complexity is bounded, independent of the underlying distribution? Unfortunately, following the so-called “no free lunch” theorem [40], the answer to the above question is negative.

In summary, a trained model  $h$  only provides probabilistic guarantee on the *expected* loss on random samples from the *underlying distribution*  $\xi$  represented by the data set  $\mathcal{D}$ . While ML models guarantee to perform well on average over the query points that follow  $\xi$ , our objective is *use-case base*, i.e., on a *single query point* – as opposed to the average performance of the model over a set of samples. A model that performs well on *majority* of samples drawn from  $\xi$  will have a high performance on average. Still, it does not necessarily mean it will perform well on the *minorities* and outlier points [11]. To further observe this, next, we shall provide an example that leads to the design of our measures.

##### 4.1 A Toy Example

As the running example in this section, let us consider the following classification task:

*Example 2* Consider a binary classification task where the input space is  $\mathbf{x} = \langle x_1, x_2 \rangle$  and the output space is the binary label  $y$  with values  $\{-1 \text{ (red)}, +1 \text{ (blue)}\}$ . Suppose the underlying data distribution  $\xi$  follows a 2D Gaussian, where  $x_1$  and  $x_2$  are positively correlated as shown in Figure 2a. The figure shows the data set  $\mathcal{D}$  drawn independently from the distribution  $\xi$ , along with their labels as their colors. Using  $\mathcal{D}$ , the prediction model  $h$  is constructed as shown in Figure 2b. The decision boundary is specified in the picture; while any point above the line is predicted as +1, a query point below it is labeled as -1. The classifier has been evaluated using a test set that is an iid sample set drawn

from the underlying data set  $\xi$ . The accuracy on the test set is high (above 90%), and hence, the model gets deployed for predicting the outcome of unseen query points. We cherry-picked four query points,  $\mathbf{q}^1$  to  $\mathbf{q}^4$ , that are also included in Figure 2b. Using  $h$  for prediction,  $h(\mathbf{q}^1) = -1$ ,  $h(\mathbf{q}^2) = +1$ ,  $h(\mathbf{q}^3) = +1$ , and  $h(\mathbf{q}^4) = -1$ . Figure 2c adds the ground-truth boundary to the search space, revealing the true label of the query points: every point inside the red circle has the true label  $-1$  while any point outside of it is  $+1$ . Looking at the figure,  $y^1 = +1$  while the model predicted it as  $h(\mathbf{q}^1) = -1$ .

Let us take a closer look at the four query points in this example and their placement with regard to the tuples in  $\mathcal{D}$  used for training  $h$ .  $\mathbf{q}^2$  belongs to a *dense region* with many training tuples in  $\mathcal{D}$  surrounding it. Besides, all of the tuples in its vicinity have the same label  $y = +1$ . As a result, one can expect that the model's outcome  $h(\mathbf{q}^2) = +1$  should be a reliable prediction. Similar to  $\mathbf{q}^2$ ,  $\mathbf{q}^4$  also belongs to a dense region in  $\mathcal{D}$ ; however,  $\mathbf{q}^4$  belongs to an *uncertain region*, where some of the tuples in its vicinity have a label  $y = +1$ , and some others have the label  $y = -1$ . Considering the uncertainty in the vicinity of  $\mathbf{q}^4$ , one cannot confidently rely on the outcome of the model  $h$ . On the other hand, the neighbors of  $\mathbf{q}^1$  (resp.  $\mathbf{q}^3$ ) are not uncertain, all having the label  $y = -1$  (resp.  $y = +1$ ). However, the query points  $\mathbf{q}^1$  and  $\mathbf{q}^3$  are not well represented by  $\mathcal{D}$ , as those would be *outlier* with respect to  $\mathcal{D}$ . In other words,  $\mathbf{q}^1$  and  $\mathbf{q}^3$  are unlikely to be generated according to the underlying distribution  $\xi$ , represented by  $\mathcal{D}$ . As a result, following the no-free-lunch theorem, one cannot expect the outcome of model  $h$  to be reliable for these points. Note that, as we observed in our experiments, model-centric techniques such as prediction intervals and conformal prediction fail to detect  $\mathbf{q}^1$  and  $\mathbf{q}^3$  as not trustworthy.

Looking at the ground-truth boundaries in Figure 2c,  $h$  luckily predicted the outcome for  $\mathbf{q}^3$  correctly, but it was not fortunate to predict the  $y^1$  correctly. Nevertheless, since the model has not reliably been trained for these outlier points, its outcome *may or may not* be accurate for these query points, hence is not trustworthy.

## 4.2 Strong and Weak Distrust Measures

From Example 2, we observe that the outcome of a model  $h$ , trained using a data set  $\mathcal{D}$  is not reliable for a query point  $\mathbf{q}$ , if:

- *Lack of representation*:  $\mathbf{q}$  is not well-presented by  $\mathcal{D}$ . In other words,  $\mathbf{q}$  is an outlier with respect to the

tuples in  $\mathcal{D}$ . In such cases, the model has not seen “enough” samples similar to  $\mathbf{q}$  to reliably learn and predict the outcome of  $\mathbf{q}$ .

- *Lack of certainty*:  $\mathbf{q}$  belongs to an uncertain region, where different tuples of  $\mathcal{D}$  in the vicinity of  $\mathbf{q}$  have different target values. In a classification context, that means the tuples have different labels (similar to  $\mathbf{q}^4$  in Example 2). Similarly, in a regression setting,  $\mathbf{q}$  belongs to a high-fluctuating area, where tuples in the vicinity of  $\mathbf{q}$  have a wide range of values on the target variable.

We design the data-centric distrust measures based on these two observations. In particular, given a query point  $\mathbf{q}$ , let  $\mathbb{P}_o$  be the probability indicating if  $\mathbf{q}$  is an outlier and let  $\mathbb{P}_u$  be the probability indicating if  $\mathbf{q}$  belongs to an uncertain region. Before formally defining the distrust measures, we would like to emphasize that our definitions are agnostic and independent from how  $\mathbb{P}_o$  and  $\mathbb{P}_u$  are computed. We still shall provide the details of how to compute these probabilities in § 5.

**Definition 1 (Strong distrust measure (SDT))** The *strong* distrust measure is a probabilistic measure that considers the outcome of a model for a query point  $\mathbf{q}$  untrustworthy if  $\mathbf{q}$  is not represented by  $\mathcal{D}$  and it belongs to an uncertain region. Formally, the strong distrust measure is:

$$\text{SDT}(\mathbf{q}) = \mathbb{P}((\mathbf{q} \text{ is outlier}) \wedge (\mathbf{q} \text{ belongs to uncertain region}))$$

Since  $\mathbb{P}_o$  and  $\mathbb{P}_u$  are independent:

$$\text{SDT}(\mathbf{q}) = \mathbb{P}_o(\mathbf{q}) \times \mathbb{P}_u(\mathbf{q}) \quad (5)$$

SDT raises the distrust warning signal only when the query point fails on *both* conditions of being represented by  $\mathcal{D}$  and not belonging to an uncertain region. For instance, in Example 2 none of the query points fail both on representation and on uncertainty; hence neither has a high SDT score. On the other hand, a high SDT score for a query point  $\mathbf{q}$  *provides a strong warning signal* that one should perhaps reject the model outcome and not consider it for decision-making.

SDT is a strong signal that raises warning only for the fearfully-concerning cases that fail both on representation and uncertainty. However, as observed in Example 2 a query points failing *at least* one of these conditions may also not be reliable, at least for critical decision making. We define the weak distrust measure to raise a warning for such cases.

**Definition 2 (Weak distrust measure (WDT))** The *weak* distrust measure is a probabilistic measure that considers the outcome of a model for a query point  $\mathbf{q}$  untrustworthy if  $\mathbf{q}$  is not represented by  $\mathcal{D}$  or it belongs

to an uncertain region. Formally, the weak distrust measure is computed as follows:

$$\begin{aligned} \text{WDT}(\mathbf{q}) &= \mathbb{P}((\mathbf{q} \text{ is outlier}) \vee (\mathbf{q} \text{ is in uncertain region})) \\ &= \mathbb{P}_o(\mathbf{q}) + \mathbb{P}_u(\mathbf{q}) - \mathbb{P}_o(\mathbf{q}) \times \mathbb{P}_u(\mathbf{q}) \end{aligned} \quad (6)$$

## 5 Implementation of the measures

### 5.1 Lack of Representation Oracle

The first component of the distrust measures identifies if the data set  $\mathcal{D}$  misses to represent the query point  $\mathbf{q}$ . The oracle returns the probabilistic measure  $\mathbb{P}_o$ , indicating if  $\mathbf{q}$  is an outlier in  $\mathcal{D}$ . Different techniques have been proposed to identify the outliers and the anomalies [16, 66, 26, 51, 19] of a data set. The distrust measures proposed in this paper are agnostic to the choice of the outlier detection technique, and alternative approaches that can compute  $\mathbb{P}_o$  are equally applicable. Still, we note that existing approaches are designed to identify the *entire set* of outliers of a given data set. Conversely, our goal is to determine if a given query point  $\mathbf{q}$  is an outlier in  $\mathcal{D}$ . As a result, those approaches are inefficient for our goal. Besides, existing approaches such as [11] often require extensive parameter tuning, and those are usually not probabilistic. Therefore, this section provides a new approach for computing the probability  $\mathbb{P}_o$ , indicating if  $\mathbf{q}$  is an outlier. In particular, we follow the existing work [11, 26, 66, 16] by considering the  $k$  nearest neighbors of  $\mathbf{q}$  in  $\mathcal{D}$  for studying if it is an outlier.

Given a distance metric  $\Delta$ , let  $\rho_{\mathbf{q}} = \Delta_k(\mathbf{q}, \mathcal{D})$  be the distance of the  $k$ -th nearest tuple in  $\mathcal{D}$  to  $\mathbf{q}$ . Considering euclidean<sup>3</sup> distance measure for  $\Delta$ ,  $\rho_{\mathbf{q}}$  is the radius of the  $k$ -vicinity of  $\mathbf{q}$ , the tight hyper-sphere (circle in 2D) centered at  $\mathbf{q}$  that includes exactly  $k$  tuples from  $\mathcal{D}$ . For example, Figure 3 shows the  $k$ -vicinity of the query points  $\mathbf{q}^1$  to  $\mathbf{q}^4$  in Example 2. It is easy to see that smaller values of  $\rho_{\mathbf{q}}$  correspond to denser  $k$ -vicinities around  $\mathbf{q}$ , meaning that the data set  $\mathcal{D}$  is more representative of the query point. We use this observation to develop the lack of representation component  $\mathbb{P}_o$ . That is, we consider the  $k$ -vicinity of  $\mathbf{q}$  and the value of  $\rho_{\mathbf{q}}$  to identify whether or not  $\mathbf{q}$  is represented by  $\mathcal{D}$ .

In particular, we would like to develop the function  $O : \mathbb{R} \rightarrow [0, 1]$  that given the value of  $\rho_{\mathbf{q}}$  returns

the probability  $\mathbb{P}_o(\mathbf{q})$ . That is,  $\mathbb{P}_o(\mathbf{q}) = O(\Delta_k(\mathbf{q}, \mathcal{D}))$ . The function  $O$  takes a distance value as the input and returns a probability indicating if the query point with that  $k$ -vicinity radius is not represented by  $\mathcal{D}$ . It is clear that as the distance values increase, the probability  $\mathbb{P}_o$  should monotonically increase as well. However, translating the distances to the probabilities is unclear and may vary from one data set to another.

Our idea is to *learn the function*  $O$  using the tuples in the data set  $\mathcal{D}$ . Specifically, we note that the probability of sampling an outlier tuple according to the underlying distribution  $\xi$  is low, and hence most of the tuples in  $\mathcal{D}$  are not outliers. Therefore, the comparison between  $\rho_{\mathbf{q}}$  and the  $k$ -vicinity radii of the tuples in  $\mathcal{D}$  can reveal if  $\mathbf{q}$  is an outlier. As a result, instead of directly translating the distance values to probabilities, we can first identify the *rank* of  $\rho_{\mathbf{q}}$  in comparison with other tuples in  $\mathcal{D}$  and use this information to specify if  $\mathbf{q}$  is an outlier. For example, if  $\rho_{\mathbf{q}}$  is smaller than more than half of  $k$ -vicinity radii of the tuples in  $\mathcal{D}$ , one can conclude that  $\mathbf{q}$  is not an outlier. On the other hand, if  $\rho_{\mathbf{q}}$  is larger than the  $k$ -vicinity radii of all tuples in  $\mathcal{D}$ , it should be an outlier.

Besides, it is often the case in practice that data sets are associated with information such as outlier ratio, showing approximately what percentage of its samples are outliers. We use such information to develop the function  $O$ .

In particular, since the ratio of the outliers in  $\mathcal{D}$  is often an estimation by the experts, we consider a Normal distribution  $\mathcal{N}(\mu, \sigma)$ , where the user-specified outlier ratio is  $(1 - \mu)$  and  $\sigma$  is the standard deviation specifying the outlier ratio estimation variance. Figure 4 demonstrates such a distribution as a bell curve centered at one minus expected outlier ratio. Note that we define the probability distribution on the *ratio of outliers in  $\mathcal{D}$*  instead of directly defining it on the distance values.

Let  $\Gamma_{\mathcal{D}}$  be the multi-set (including duplicate values) of  $k$ -vicinity radii of the tuples in  $\mathcal{D}$ . Let  $r_{\mathbf{q}}$  be the percentage of values in  $\Gamma_{\mathcal{D}}$  that are not larger than  $\Delta_k(\mathbf{q}, \mathcal{D})$ . That is

$$r_{\mathbf{q}} = \frac{|\{r \in \Gamma_{\mathcal{D}} | r \leq \Delta_k(\mathbf{q}, \mathcal{D})\}|}{n} \quad (7)$$

The query point  $\mathbf{q}$  is an outlier if its  $k$ -vicinity radius falls within the range of outlier radii. That is, if the boundary of outlier values in  $\Gamma_{\mathcal{D}}$  is smaller than  $r_{\mathbf{q}}$ ,  $\mathbf{q}$  is considered an outlier. Now to compute the probability  $\mathbb{P}_o(\mathbf{q})$ , the function  $O$  can use the probability distribution  $\mathcal{N}(\mu, \sigma)$ . As shown in Figure 4,  $\mathbb{P}_o(\mathbf{q})$  is the probability that the outlier boundary  $r$  is less than or equal to  $r_{\mathbf{q}}$ , i.e.  $\mathbb{P}_o(\mathbf{q}) = \mathbb{P}(r \leq r_{\mathbf{q}})$ .

<sup>3</sup> Please note that while we use euclidean distance for the explanation and examples in the paper, our metrics and algorithms are agnostic to the choice of the distance measure, and those equally work for other ones. We evaluate the impact of the choice of the distance measure (using multiple well-known measures) in our experiments. Our experiments show consistent results across different measures.

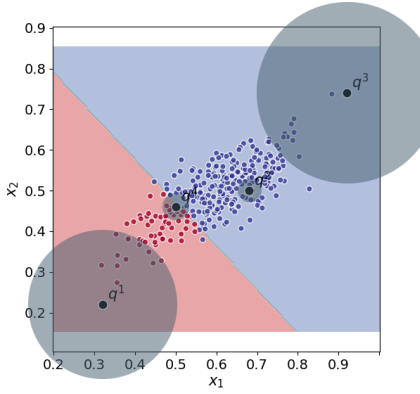


**Fig. 3:** Illustration of the  $k$ -vicinity ( $k = 10$ ) of  $\mathbf{q}^1$  to  $\mathbf{q}^4$  in Example 2.

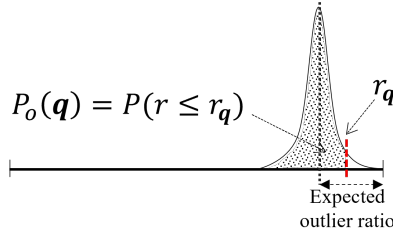


**Fig. 4:** Computation of  $\mathbb{P}_o(\mathbf{q})$  using the ratio of tuples in  $\mathcal{D}$  with smaller  $k$ -vicinity radius than  $\Delta_k(\mathbf{q}, \mathcal{D})$ .

id	$x_1$	$x_2$	2-NN	$\rho$
$t^1$	0.61	0.58	$\{t^5, t^6\}$	0.191
$t^2$	0.32	0.77	$\{t^7, t^9\}$	0.161
$t^3$	0.79	0.41	$\{t^1, t^5\}$	0.247
$t^4$	0.13	0.9	$\{t^7, t^{10}\}$	0.082
$t^5$	0.74	0.44	$\{t^1, t^3\}$	0.191
$t^6$	0.55	0.64	$\{t^1, t^9\}$	0.183
$t^7$	0.18	0.85	$\{t^4, t^{10}\}$	0.147
$t^8$	0.93	0.12	$\{t^3, t^5\}$	0.372
$t^9$	0.38	0.71	$\{t^2, t^6\}$	0.183
$t^{10}$	0.05	0.92	$\{t^4, t^7\}$	0.147

**Fig. 5:** The data set in Example 3.

Converting the values to the standard-Normal distribution and using the  $Z$ -table:

$$\mathbb{P}_o(\mathbf{q}) = \mathbb{P}(r \leq r_{\mathbf{q}}) = \mathcal{Z}\left(\frac{r_{\mathbf{q}} - \mu}{\sigma}\right) \quad (8)$$

To further elaborate on how  $\mathbb{P}_o(\mathbf{q})$  is computed, let us consider the following example:

*Example 3* Consider the 2D data set  $\mathcal{D}$  with  $n = 10$  tuples shown in the table of Figure 5. In addition to the tuple values on  $x_1$  and  $x_2$ , the table also includes the  $k$ -NN ( $k = 2$ ) of the tuples and the radius  $\rho$  of their  $k$ -vicinity. Let the outlier ratio of the data set be 20% ( $\mu = 1 - 0.2 = 0.8$ ) with a standard deviation of  $\sigma = 0.1$ . Now consider the query point  $\mathbf{q} : \langle 0.81, 0.76 \rangle$ . The 2-NN of  $\mathbf{q}$  are  $\{t_1, t_6\}$ , and  $\rho_{\mathbf{q}} = 0.286$ . Looking at the last column of Figure 5, only  $t^8$  has a larger  $k$ -vicinity radius than  $\rho_{\mathbf{q}}$ , i.e., for 90% of tuples the  $k$ -vicinity radius is smaller than  $\rho_{\mathbf{q}}$ . Therefore, using Equation 8,  $\mathbb{P}_o(\mathbf{q}) = \mathcal{Z}((0.9 - 0.8)/0.1) = 0.84$ .

Computing Equation 8 requires (i) computing  $\Delta_k(\mathbf{q}, \mathcal{D})$ , which requires finding the  $k$ -NN of  $\mathbf{q}$ , and (ii) computing the value of  $r_{\mathbf{q}}$ . The baseline approach for computing these values makes a linear pass over  $\mathcal{D}$  to identify the  $k$ -NN of  $\mathbf{q}$ . Besides, it requires  $O(n^2)$  to compute the multi-set of  $k$ -vicinity radii  $\Gamma_{\mathcal{D}}$  for the tuples in  $\mathcal{D}$  and then it needs  $O(n)$  to make a pass over  $\Gamma_{\mathcal{D}}$  to compute  $r_{\mathbf{q}}$ .

However, given the interactive nature of query answering for ML systems and potentially large size of  $\mathcal{D}$ , we are interested in designing an algorithm that runs in a *sublinear* time to  $n$ . Theoretically speaking, finding the  $k$  nearest neighbors of a point can be done in  $O(\log n)$  using  $k$ -voronoi diagrams<sup>4</sup> [21, 5, 49, 14], while

<sup>4</sup>  $k$ -voronoi diagram is a partitioning of the query space into convex cells where the  $k$ -NN of all points in each cell is the same set of tuples.

### Algorithm 1

**Input:** data set  $\mathcal{D}$ ;  $k$ ; expected outlier ratio  $\tau$ ; standard deviation  $\sigma$ ; query point  $\mathbf{q}$

- 1: **function** PREPROCESS $_o(\mathcal{D}, k)$
- 2:    $M \leftarrow$  build the  $k$ -NN index of  $\mathcal{D}$ ;  $\Gamma \leftarrow []$
- 3:   **for**  $t \in \mathcal{D}$  **do**
- 4:      $V \leftarrow k\text{-NN}(t)$
- 5:     add  $\max_{t' \in V} \Delta(t, t')$  to  $\Gamma$
- 6:   **return**  $M$ ,  $\text{sort}(\Gamma)$
- 7: **function**  $\mathbb{P}_o(\mathbf{q})$
- 8:    $\rho_{\mathbf{q}} \leftarrow \max \Delta(\mathbf{q}, t'), \forall t' \in k\text{-NN}(\mathbf{q}, M)$
- 9:    $r_{\mathbf{q}} \leftarrow \frac{1}{n} \text{BINARYSEARCH}(\rho_{\mathbf{q}}, \Gamma)$
- 10: **return**  $\mathcal{Z}\left(\frac{r_{\mathbf{q}} - \mu}{\sigma}\right)$

constructing the  $k$ -voronoi cells takes polynomial time for a constant number of dimensions [5, 25] ( $O(k^2 n \log n)$  for 2D [49]). Besides, practically efficient algorithms have been proposed [37, 84, 77], construct data structures in preprocessing time that enables identifying  $k$ -NN is near-logarithmic time. We rely on the off-the-shelf techniques for finding the  $k$ -NN of a query point.

During the preprocessing time, we first construct the  $k$ -NN data structure. Next, for every tuple in  $\mathcal{D}$ , we identify its  $k$ -vicinity radius and add it to the list  $\Gamma_{\mathcal{D}}$ . Finally, to quickly identify the value of  $r_{\mathbf{q}}$  in query time, we sort the list  $\Gamma_{\mathcal{D}}$ .

The preprocessing algorithm and the function for identifying  $\mathbb{P}_o(\mathbf{q})$  are provided in Algorithm 1. To compute  $r_{\mathbf{q}}$  for a query point  $\mathbf{q}$ , the algorithm first finds the  $k$ -vicinity of  $\mathbf{q}$  and identifies the tuple in  $k$ -vicinity with maximum distance from  $\mathbf{q}$ . Next, it applies a binary search on the sorted list  $\Gamma$  to identify the number of cells in  $\Gamma$  that have a value not larger than  $\mathbf{q}$ , and use it to compute  $r_{\mathbf{q}}$ . At last, it uses Equation 8 and returns the value of  $\mathbb{P}_o(\mathbf{q})$ .

Let  $T_{c_n}$  be the time to construct the  $k$ -NN index. Also, let  $T_{q_n} \simeq O(\log n)$  be the time to identify the  $k$ -

NN of a query point, using the constructed index. The preprocessing function constructs the  $k$ -NN index, identifies the  $k$ -NN of each tuple in  $\mathcal{D}$ , and finally spends  $O(n \log n)$  to sort the list  $\Gamma$ . Therefore, the total preprocessing time is  $O(T_{c_n} + n^2)$ . Computing  $\mathbb{P}_o(\mathbf{q})$  requires  $T_{q_n}$  to identify the  $k$ -NN of  $\mathbf{q}$  and  $O(\log n)$  for the binary search. As a result, the time to compute  $\mathbb{P}_o(\mathbf{q})$  is  $O(T_{q_n} + \log n) \simeq O(\log n)$ .

## 5.2 Lack of Certainty Oracle

After the lack of representation oracle, we now turn our attention to the uncertainty oracle that, given the query point, the data set  $\mathcal{D}$ , and the target variable  $y$ , returns  $\mathbb{P}_u$ , the probabilistic measure that indicates if  $\mathbf{q}$  belongs to an uncertain region. There has been extensive research, and there exist different metrics for computing uncertainty, namely, entropy, Gini impurity, Brier score, and probability calibration [72, 15, 17, 62, 30]. Indeed, we are agnostic to the choice of the technique for developing the uncertainty oracle, and any method that can compute the probabilistic measure  $\mathbb{P}_u$  is equally applicable. Even so, in the rest of this section, we provide a development of the uncertainty oracle, following the technique proposed in § 5.1. Similar to § 5.1, we use the  $k$ -vicinity of a query point  $\mathbf{q}$  as the region for studying uncertainty.

Binary classification is among the most popular ML tasks. A straightforward approach for developing the uncertainty oracle for such cases is to use the *Shannon entropy* ( $\mathcal{H}$ ) [72]. Let  $v_1, \dots, v_\ell$  be the set of possible values for a target variable  $y$ . Known as a measure of uncertainty, the entropy of the random variable  $y$  is

$$\mathcal{H}(y) = - \sum_{\ell=1}^{\ell} \mathbb{P}(v_\ell) \log \mathbb{P}(v_\ell) \quad (9)$$

Higher entropy values refer to higher uncertainty, while values close to zero indicate a high certainty in the value of  $y$ . For a binary variable  $y$ , the maximum value of entropy is one, and it refers to the cases where the probability of each value is 0.5. Using entropy to measure uncertainty for binary classification, we consider the set of tuples  $V_k(\mathbf{q}) \subseteq \mathcal{D}$  in the  $k$ -vicinity of the query point  $\mathbf{q}$  and compute  $\mathbb{P}_u(\mathbf{q})$  as the entropy among them. Let  $p_1$  be the ratio of tuples in  $V_k(\mathbf{q})$  with label 1. Then,

$$\mathbb{P}_u(\mathbf{q}) = -p_1 \log p_1 - (1 - p_1) \log(1 - p_1) \quad (10)$$

Entropy can also be used for non-binary classification. However, when the cardinality of  $y$  is larger than 2, entropy is not bounded by 1 anymore. While different approaches can be applied for transforming the entropy values to probabilistic measures, we choose a method

similar to our proposal in § 5.1. That is, we use the uncertainty values in  $k$ -vicinities of the tuples in  $\mathcal{D}$  as an indicator showing if  $\mathbf{q}$  belongs to an uncertain region. Assuming that a model trained using  $\mathcal{D}$  has high accuracy (or it will not get deployed in practice), one can conclude if the model should perform well for a query point that its uncertainty is comparable with the uncertainty of the tuples in  $\mathcal{D}$ . In other words, one can identify the tuples in  $\mathcal{D}$  that their uncertainty is considered outlier compared to other tuples in the data set. Let  $r_u$  be the expected percentage of the tuples in  $\mathcal{D}$  that have an uncertain  $k$ -vicinity. We consider a Normal distribution  $\mathcal{N}(\mu_u, \sigma_u)$  where  $\mu_u = (1 - r_u)$  and  $\sigma_u$  is the standard deviation of uncertain ratio estimation. During the preprocessing, we construct  $\Gamma_{u\mathcal{D}}$ , the sorted list of uncertainty values for the tuples in  $\mathcal{D}$ . Then, given a query point  $\mathbf{q}$ , we first compute  $\mathcal{H}_{\mathbf{q}}(y)$ , the uncertainty in the  $k$ -vicinity of  $\mathbf{q}$  using Equation 9. Next, applying a binary search on  $\Gamma_{u\mathcal{D}}$ , we compute  $r_{u\mathbf{q}}$ , the ratio of uncertainty values in  $\Gamma_{u\mathcal{D}}$  that are not larger than  $r_{u\mathbf{q}}$ . Finally, converting the values to standard-Normal distribution,  $\mathbb{P}_u(\mathbf{q})$  is computed as following:

$$\mathbb{P}_u(\mathbf{q}) = \mathbb{P}(r \leq r_{u\mathbf{q}}) = \mathcal{Z}\left(\frac{r_{u\mathbf{q}} - \mu_u}{\sigma_u}\right) \quad (11)$$

The residual sum of squares (RSS) is a popular measure for regression. In regression trees [15], for example, the objective is to split the search space into regions with high certainty, where the RSS values in each region are minimized, i.e., the certainty in each region is maximized. We also use RSS for measuring  $\mathbb{P}_u(\mathbf{q})$  for the regression tasks. Let  $V_k(\mathbf{q}) \subseteq \mathcal{D}$  be the set of tuples in the  $k$ -vicinity of  $\mathbf{q}$ . Also, let  $m_{u\mathbf{q}}$  be the average of  $y$  values in  $V_k(\mathbf{q})$ . That is,  $m_{u\mathbf{q}} = (\sum_{\mathbf{t}^i \in V_k(\mathbf{q})} y^i) / k$ . Then the uncertainty around  $\mathbf{q}$  is computed as

$$rss_{\mathbf{q}}(y) = \sum_{\mathbf{t}^i \in V_k(\mathbf{q})} (y^i - m_{u\mathbf{q}})^2 \quad (12)$$

The process for computing  $\mathbb{P}_u(\mathbf{q})$  is the same as the one for classification, with the only difference being that RSS should be used for computing uncertainty (instead of entropy).

The pseudo-code of the function  $\mathbb{P}_u(\mathbf{q})$ , along with preprocessing steps, are provided in Algorithm 2. Following a similar procedure as of Algorithm 1, the time to compute  $\mathbb{P}_u(\mathbf{q})$  is  $O(T_{q_n} + \log n) \simeq O(\log n)$ . Using the functions  $\mathbb{P}_o$  and  $\mathbb{P}_u$ , it takes a (near) logarithmic time to compute the uncertainty measures STD and WDT.

## 5.3 No Data Access During the Query Time

During the query answering phase, Algorithms 2 and 1 require to compute the  $k$ -vicinity radius and the en-

**Algorithm 2**


---

**Input:** data set  $\mathcal{D}$ ;  $k$ ; expected uncertainty ratio  $r_u$ ; standard deviation  $\sigma_u$ ; query point  $\mathbf{q}$ ;  $k$ -NN index  $M$

```

1: function UNCERTAINTY( $V$ )
2:   if  $y$  is categorical /*classification*/ then
3:      $r_\ell \leftarrow |\{t^i \in V | y^i = v_\ell\}| / k, \forall v_\ell \in \text{Dom}(y)$ 
4:   return  $-\sum_{i=1}^{\ell} r_\ell \log(r_\ell)$ 
5:    $m_u \leftarrow (\sum_{t^i \in V} y^i) / k$ 
6:   return  $\sum_{t^i \in V} (y^i - m_u)^2$ 
7: function PREPROCESS $_u(\mathcal{D}, k)$ 
8:    $\Gamma_u \leftarrow []$ 
9:   for  $t \in \mathcal{D}$  do add UNCERTAINTY( $k$ -NN( $t$ )) to  $\Gamma_u$ 
10:  return sort( $\Gamma_u$ )
11: function  $\mathbb{P}_u(\mathbf{q})$ 
12:    $u_{\mathbf{q}} \leftarrow \text{UNCERTAINTY}(k\text{-NN}(\mathbf{q}, M))$ 
13:    $r_{\mathbf{q}} \leftarrow \text{BINARYSEARCH}(u_{\mathbf{q}}, \Gamma_u) / n$ 
14:  return  $\mathcal{Z}(\frac{r_{\mathbf{q}} - \mu_u}{\sigma_u})$ 
15: function SDT( $\mathbf{q}$ ) return  $\mathbb{P}_o(\mathbf{q}) \times \mathbb{P}_u(\mathbf{q})$ 
16: function WDT( $\mathbf{q}$ )
17:    $p_1 \leftarrow \mathbb{P}_o(\mathbf{q}); p_2 \leftarrow \mathbb{P}_u(\mathbf{q})$ 
18:  return  $p_1 + p_2 - p_1 \times p_2$ 

```

---

trophy with the  $k$ -NN of a query point  $q$ . Although off-the-shelf  $k$ -NN indices are used to find this information, one could view it as requiring to access the training data after preprocessing. Our practical approach to address this is to *learn* these values. That is, to create two models that take as the input a query point as the input, returning the  $k$ -vicinity radii and the entropy values. Creating these models requires sampling from the query space, i.e., to generate a large-enough training set with observations being i.i.d samples from the query space, while the target variables are the  $k$ -vicinity radius and entropy. On the positive side, one can generate an arbitrarily large training set by generating i.i.d sample queries and then computing the target values using their  $k$ -NN. On the flip side, however, as proven in [11], the theoretical upper bound on the number of samples needed is exponential. In other words, theoretically speaking, the size training set may need to be exponential in  $d$  for adversarial cases, in order to guarantee a given error  $\varepsilon$ . Fortunately, as we observe in our experiments, the theoretical upper bound is not tight, and in practice, the training set size is much smaller.

We still need to specify the proper training set size for our learning tasks. To do so, we design an *exponential search* algorithm as follows: the algorithm starts by setting the sample set size  $N_s$  to an initial value ( $O(n)$ ). It then collects  $N_s$  i.i.d samples  $\mathcal{S}$  from the query space and finds the  $k$ -vicinity of each sample  $s_i$  and identifies the  $k$ -vicinity radius<sup>5</sup> of  $s_i$  as  $\rho_i \leftarrow \max \Delta(s_i, t'), \forall t' \in k\text{-NN}(s_i)$ . Next, the algorithm builds

<sup>5</sup> The process to learn the entropy values is the same as learning the  $k$ -vicinity radii.

a regression model  $\mathcal{M}$  using  $\mathcal{S}$  as the training set. After building the model, the algorithm checks if  $\mathcal{M}$  has the error of at most  $\varepsilon$ , for a user-specified error  $\varepsilon$ . To check this, the model uses the test set  $\mathcal{T}$ . If  $\text{error} > \varepsilon$ , the algorithm *doubles the sample size* and repeats the process until it reaches the right sample size for  $N_s$ .

Let  $\text{Reg}_\rho$  and  $\text{Reg}_U$  be the trained regression models that return the  $k$ -vicinity radius and the  $k$ -NN entropy of a query point  $\mathbf{q}$ , respectively. Then, the only changes in the proposed algorithms are (i) replace Line 8 of Algorithm 1 with  $\rho_{\mathbf{q}} \leftarrow \text{Reg}_\rho(\mathbf{q})$  and (ii) replace Line 8 of Algorithm 2 with  $u_{\mathbf{q}} \leftarrow \text{Reg}_U(\mathbf{q})$ .

## 6 Parameter Tuning

Similar to many other techniques in data mining and ML, the distrust measures require parameter tuning. In implementing distrust measures, we take the neighborhood size  $k$  in  $k$ -NN, along with the outlier ratio  $c$  of the training samples, the uncertainty ratio  $u$ , and the standard deviation for uncertainty and outlier distributions as hyper-parameters. The techniques proposed in this paper are agnostic to the choice of parameter tuning. Nevertheless, in this section, we present some heuristics for tuning these parameters.

### 6.0.1 Tuning Neighborhood Size and Outlier Ratio Parameters

The first parameter to determine is  $k$ : the number of tuples in  $\mathcal{D}$  that specify the vicinity of the queried point. The second parameter is the outlier ratio  $c$ , which estimates the percentage of the tuples in the data set that are outliers.

To jointly tune  $c$  and  $k$  for a data set  $\mathcal{D}$ , we adopt a technique proposed in [85] for tuning the parameters of the local outlier factor (LOF) [16] algorithm. However, instead of choosing top  $\lfloor cn \rfloor$  points with the highest LOF scores, we select top  $\lfloor cn \rfloor$  with the highest  $k$ -vicinity radii.

We define a grid of values for  $c$  and  $k$ . For each combination, we calculate the  $k$ -vicinity radius for all tuples in  $\mathcal{D}$ , choose the top  $\lfloor cn \rfloor$  tuples as the outliers, and the top  $\lfloor cn \rfloor$  of remaining tuples as the inliers. The inliers are chosen in this manner because we are only interested in the tuples that are most similar to the outliers.

For each  $c$  and  $k$ , now we have a list of  $k$ -vicinity radii for outliers and a list for inliers and we calculate mean ( $\mu_{out}(c, k), \mu_{in}(c, k)$ ) and variance ( $\sigma_{out}^2(c, k), \sigma_{in}^2(c, k)$ ) over the log of the values in each list. We define the standardized difference in mean log  $k$ -vicinity radii between the outliers and the inliers as

$$T_{c,k} = \frac{\mu_{out}(c,k) - \mu_{in}(c,k)}{\sqrt{[cn]^{-1}(\sigma_{out}^2(c,k) + \sigma_{in}^2(c,k))}}$$

If  $c$  is known, it is enough to find  $k_c^* = \arg \max_k T_{c,k}$  that maximizes the standardized difference between the outliers and inliers for the corresponding  $c$ . Otherwise, we assume that  $k$ -vicinity radii form a random sample following a Normal distribution with the mean  $\mu_{out}(c)$  and variance  $\sigma_{out}^2(c)$  for outliers, and one with mean  $\mu_{in}(c)$  and variance  $\sigma_{in}^2(c)$  for the inliers. Then given a value of  $c$ ,  $T_{c,k}$  approximately follows a non-central  $t$  distribution with degrees of freedom  $df_c = 2[cn] - 2$  and the non-centrality parameter:

$$ncp_c = \frac{\mu_{out}(c) - \mu_{in}(c)}{\sqrt{[cn]^{-1}(\sigma_{out}^2(c) + \sigma_{in}^2(c))}}$$

We cannot directly compare the largest standardized difference  $T_{c,k_c^*}$  across different values of  $c$  because  $T_{c,k}$  follows different non-central  $t$  distributions depending on  $c$ . Instead, we can compare the quantiles that correspond to  $T_{c,k_c^*}$  in each respective non-central distribution so that the comparison is on the same scale. To do so, we define  $c_{opt} = \arg \max_c P(z < T_{c,k_c^*}; df_c; ncp_c)$ , where the random variable  $z$  follows a non-central  $t$  distribution with  $df_c$  degrees of freedom and  $ncp_c$  non-centrality parameter.  $c_{opt}$  is where  $T_{c,k_c^*}$  is the largest quantile in the corresponding  $t$  distribution as compared to the others.

### 6.0.2 Tuning Uncertainty Ratio Parameter

The next parameter we need to tune is the uncertainty ratio  $u$ , which estimates what percentage of data belongs to uncertain regions. Similar to the outliers ratios that help us transform the  $k$ -vicinity radii to probabilities, the expected uncertainty ratio  $u$  helps us transform an uncertainty value in a  $k$ -vicinity to a probability. We consider the distribution of uncertainty values within the  $k$ -vicinity of tuples in  $\mathcal{D}$  for identifying  $u$ . To explain the intuition behind this choice, let us consider a classification task. While the uncertainty for the tuples far from the decision boundary should be low, the uncertainty suddenly increases as one gets close to the boundary. As a result, looking at the distribution of uncertainty values, one should be able to identify an estimation of  $u$  by finding the sharp slope in the distribution of uncertainty values. Following this intuition, we calculate the  $k$ -vicinity uncertainty for each tuple in  $\mathcal{D}$ , and create the reverse cumulative distribution  $V: [0, 1] \rightarrow \mathbb{R}$  such that, for every value  $r$ , the ratio of tuples in  $\mathcal{D}$  with an uncertainty value larger than  $V(r)$

is  $r$ . For example,  $V(0.1)$  returns the value  $u_{0.1}$  such that the uncertainty for 10% of tuples is larger than it. We then identify the knee of this function (the sharp decrease in  $V(r)$ ) as the estimated uncertainty ratio. As a rule of thumb in our experiments, we observe that the knee falls around 10-15%.

## 7 Experiments

We conduct comprehensive experiments on multiple synthetic and real-world data sets of diverse sizes and dimensions using a variety of models (Logistic Regression, K-Nearest-Neighbor, Artificial Neural Networks, Deep Neural Networks, ElasticNet, Random Forest, and SVM), distance measures (Braycurtis, Canberra, Chebyshev, Cityblock, Manhattan and Euclidean), and tasks (regression and binary/multi-class classification including text classification and image processing) to validate the effectiveness and consistency of our proposal and evaluate the efficiency and scalability of our algorithms. We also demonstrate the failure of existing work such as Conformal Prediction, Prediction Probabilities (for cases that are not represented by the data), and data coverage (for the cases that belong to the uncertain regions) and how our proposed measures perform superior in capturing the prediction unreliability associated with point queries.

### 7.1 Experiments Setup

The experiments were conducted using a 2.5 GHz Quad-Core Intel Core i7 processor, 16 GB memory, and running macOS. The algorithms were implemented in Python.

#### 7.1.1 Data Sets

For evaluation purposes, we used (i) a collection of synthetic data sets and (ii) *seven real-world data sets* for regression and binary/multi-class classification including text and image classification.

**Challenge:** In the evaluation of our distrust measures, we needed to generate samples with different distrust values. However, since the tuples with high distrust values are unlikely to be drawn from the underlying distribution  $\xi$ , it is challenging to collect enough samples (as a test set) to evaluate the effectiveness of our measures. A comprehensive evaluation requires query points drawn uniformly from the query space to cover different parts of it. To achieve this, we need to have access to a ground truth oracle that for *any* given sample taken from the query space returns the value of



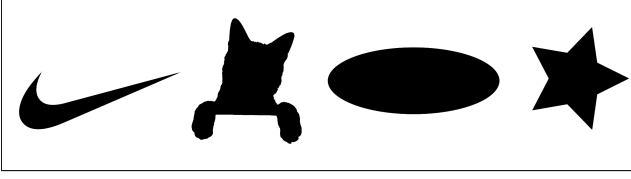


**Fig. 6:** Shapes used as the ground truth in creating the synthetic data sets *SYN*

*target variable*. However, finding a real-world data set in a context where the ground truth oracle exists (publicly) is challenging. To overcome this challenge, we take three directions: first, to have full control of the shape and complexity of the ground truth labels over different data sets, we generate synthetic data; second, we find a real-world data set and a third party (public) service that provides access to ground truth labels; and third, we find a very large data set that contains samples from different parts of the query space and apply sub-sampling on it. Next, we remove the outliers from each sample and split each cleaned sample into train and test sets, and add the outliers to the test set to cover larger parts of the query space.

**Real Data Sets:** We use multiple real data sets, as briefly explained in the following:

1. **3D Road Network (RN) Data set [41]** is a benchmark data set for **regression** that was constructed by adding elevation information to a 2D road network in North Jutland, Denmark. It includes 434,874 records with attributes `Latitude`, `Longitude`, and `Altitude`. We took 30 samples of size 10,000 from *RN* data set and generated 30 data sets and repeated each experiment 30 times, using different data sets. To address the evaluation challenge for the *RN* data set, we generated a uniform sample of 6,400 points  $\langle x_1, x_2 \rangle$  in the range  $[0, 1]$ . We then transform the uniform samples back to the same space as the points in *RN*. Then, we used an *off-the-shelf API*<sup>6</sup> that given every coordinate  $\langle \text{Latitude}, \text{Longitude} \rangle$  in the data space, it yields the corresponding `Altitude` as the oracle to obtain the ground truth values.
2. **House Sales in King County (HS) Data set [35]** is a **regression** data set for house sale prices for King County (Seattle). It includes houses sold between May 2014 and May 2015. It includes 21,614 records having 21 attributes with 2 categorical and 16 continuous types. Given attributes such as `no. of bedrooms`, `square footage`, `floors`, etc., the task is to predict the `price` of the house. We took

30 samples of size 10,000 from *HS* data set, generated 30 data sets, and repeated each experiment 30 times, using different data sets. To address the evaluation challenge for *HS* data set, for each sample, we removed the outliers and then split the data set into train and test sets. We then added the outliers back to the test set. Although with *HS* we can not measure the distrust values for the whole query space, we believe the findings can still confirm the effectiveness of our measures.

3. **Diamond (DI) Data set [6]** is a **regression** data set for predicting the price of diamond given some visual properties. This data set has 53,941 records with 14 attributes, 6 of which are continuous and 3 categorical. We used a similar approach to *HS* data set for utilizing *DI* in our experiments.
4. **Default of Credit Card Clients (DCC) Data set [86]** is a data set for **classification** that was constructed from payment data in October 2005 from an important bank in Taiwan. The data set is binary class with – default payment (Yes = 1, No = 0), as the response variable. Among the 30,000 records, 6,636 (22.12%) are the cardholders with default payment. The data set has 23 features (9 categorical and 14 continuous) including `credit line`, `age`, `gender`, `education`, `history of payment`, `amount of bill statement`, `amount of the previous statement`, etc. Since it was not feasible for us to devise a function that can produce the ground truth for *DCC*, we took a sample of size 15,000 from the data set and then split it into two sets of train (5,000 tuples) and test (10,000 tuples) and used the test set as a substitute for the uniform sample over the query space. Following the same procedure, we generated 30 data sets and repeated each experiment 30 times, using different data sets. Similar to *HS*, we can not measure the distrust values for the whole query space in *DCC*, yet the findings can still confirm the effectiveness of our measures.
5. **Adult (AD) Data set [45]** is a well-known benchmark data set for **classification** tasks predicting whether income exceeds \$50K annually based on census data. This data set has 32,561 records with 14 attributes, 6 of which are continuous and 8 categorical. We used a similar approach to the *HS* data set for utilizing *AD* in our experiments.
6. **Real-sim (RS) Data set [54]** is based on *SRAA*[55] data set, preprocessed for SVMlin project [73]. The data set is designed for **text classification** tasks and is based on UseNet articles of four discussion groups on simulated auto racing, simulated aviation, real autos, and real aviation. The task is to separate real data from simulated data. *RS* is a sparse data

<sup>6</sup> <https://api.open-elevation.com/>

set and has 72,309 records with 20,958 attributes with continuous values. We used a similar approach to *HS* data set for utilizing *RS* in our experiments.

7. **Gisette (GS) Data set [34]** is a handwritten digit recognition data set based on the popular *MNIST* data set [48] for **image classification** to separate highly confusable digits ‘4’ and ‘9’. The digits have been size-normalized and centered in a fixed-size image of  $28 \times 28$  pixels. This data set has 6,000 records with 5,000 attributes with continuous values. We used a similar approach to *HS* data set for utilizing *GS* in our experiments.

**Synthetic (SYN) Data Sets:** To fully investigate the relationship between the distrust measures and the model performance, we generated a collection of 60 data sets and repeated each experiment 60 times, using different data sets. Each data set is a random sample following a 2D Gaussian distribution with  $\mu = [0, 0]$  and  $\Sigma = \begin{bmatrix} 6 & 4 \\ 3 & 1 \end{bmatrix}$  over the input space  $\mathbf{x} = \langle x_1, x_2 \rangle$  where  $x_1$  and  $x_2$  are positively correlated and the output space is the binary label  $y$  with values  $\{-1, +1\}$ . To create the binary classes for each data set, we randomly moved the samples over each shape in Figure 6 in a way that the sample and shape have an intersection. As a result, each shape is the ground truth for 15 data sets but with different placements. A data point belongs to the  $-1$  class, if it falls into the corresponding shape, otherwise, it belongs to the  $+1$  class. To address what we discussed in the evaluation challenge, we create a uniform sample of size 6,400 over  $[0, 1]$  and will label the points with respect to each shape and its placement in the space, generating a total of 60 uniform samples corresponding to each data set. In particular, following Example 2, we consider a binary classification task over the observation variables  $x_1$  and  $x_2$ . We chose a 2D setting for visualization purposes.

All continuous values used are normalized in the range  $[0, 1]$ , using  $(v_i - \min)/(\max - \min)$  and the non-ordinal ones are one-hot encoded using scikit-learn OneHotEncoder.

**Default values:** To evaluate the performance of our algorithms under different settings, we vary the value of a parameter, while fixing the value of the other ones. The default value for neighborhood size  $k$  is 10. The outlier ratio  $c$  is set to 0.1 suggesting that a mean  $\mu = 0.9$  is chosen for outlier distribution with a standard deviation  $\sigma = 0.1$ . We adopt a technique proposed in [85] to jointly tune  $k$  and  $c$  parameters for a given data set. The tuning procedure for these two parameters alongside uncertainty ratio parameter  $u$  is discussed in detail in section 6. The default value for  $d$  (number of at-

tributes) is 2 for *SYN* and *RN* data sets, while it is 20, 18, 9, 14, 6,000, and 20,958 for *DCC*, *HS*, *DI*, *AD*, *GS* and *RS* respectively. The default value of  $n$  (size of data set) for the *SYN*, *RN*, *HS*, *DCC*, *DI*, *AD*, *GS* and *RS* data sets are 1,000, 10,000, 10,000, 5,000, 43,150, and 32,560, 6,000 and 72,309. The uncertainty ratio  $u$  is set to 0.1, therefore, a mean  $\mu_u = 0.9$  is chosen for uncertainty distribution with a standard deviation  $\sigma_u = 0.1$ .

## 7.2 Proof of Concept

We start our experiments by evaluating the effectiveness of distrust measures across different data sets, ML models, and different parameters. Since the distrust measures are task-independent, we perform the effectiveness validation experiments for both classification and regression tasks. For the classification tasks, we use *SYN*, *DCC*, *AD*, *RS* and *GS* data sets, and for the regression tasks, we employ *RN*, *HS* and *DI* data sets. To demonstrate the effectiveness of the distrust measures we first provide a visual validation, using one of the 2D *SYN* data sets. We then present a comprehensive validation over all our data sets by providing the correlation between the distrust values and the performance of an ML model’s prediction on the same data. To do so, we deliver the results as bar graphs in which the  $x$ -axis is a bucketization of the ranges of the distrust measures and the  $y$ -axis is the ML model’s evaluation score. Each bar represents a value corresponding to a measure of accuracy/error i.e. *Accuracy*, *F1 score*, *FPR* and *FNR* of the ML model for all the tuples that have a distrust value in the same range as the bar.

**Visual validation:** Consider the 2D data set  $\mathcal{D}$  shown in Figure 7a.  $\mathcal{D}$  is borrowed from *SYN* as one of the 60 data sets with the shape of the cat as the ground truth (we obtained similar results for other data sets, as reflected in the aggregate values we shall report next). We compute SDT and WDT values for each query point in the uniform sample over the space using the default settings. In Figures 7b and 7c, the query space is colored by assigning a tone based on the corresponding values of SDT and WDT respectively. As shown in Figure 7b, the untrustworthy regions are the set of query points in the space that are both outliers with respect to the tuples in  $\mathcal{D}$  and also uncertain since the entropy in their  $k$ -vicinity is high. On the other hand, in Figure 7c, the untrustworthy regions are the set of query points that are either outliers or uncertain. The closer the color to red, the more untrustworthy the region will be and the opposite goes for green. Next, we train an arbitrary classifier (LR in this case) on data set  $\mathcal{D}$  and evaluate the model’s prediction. In this regard, we bucketize the

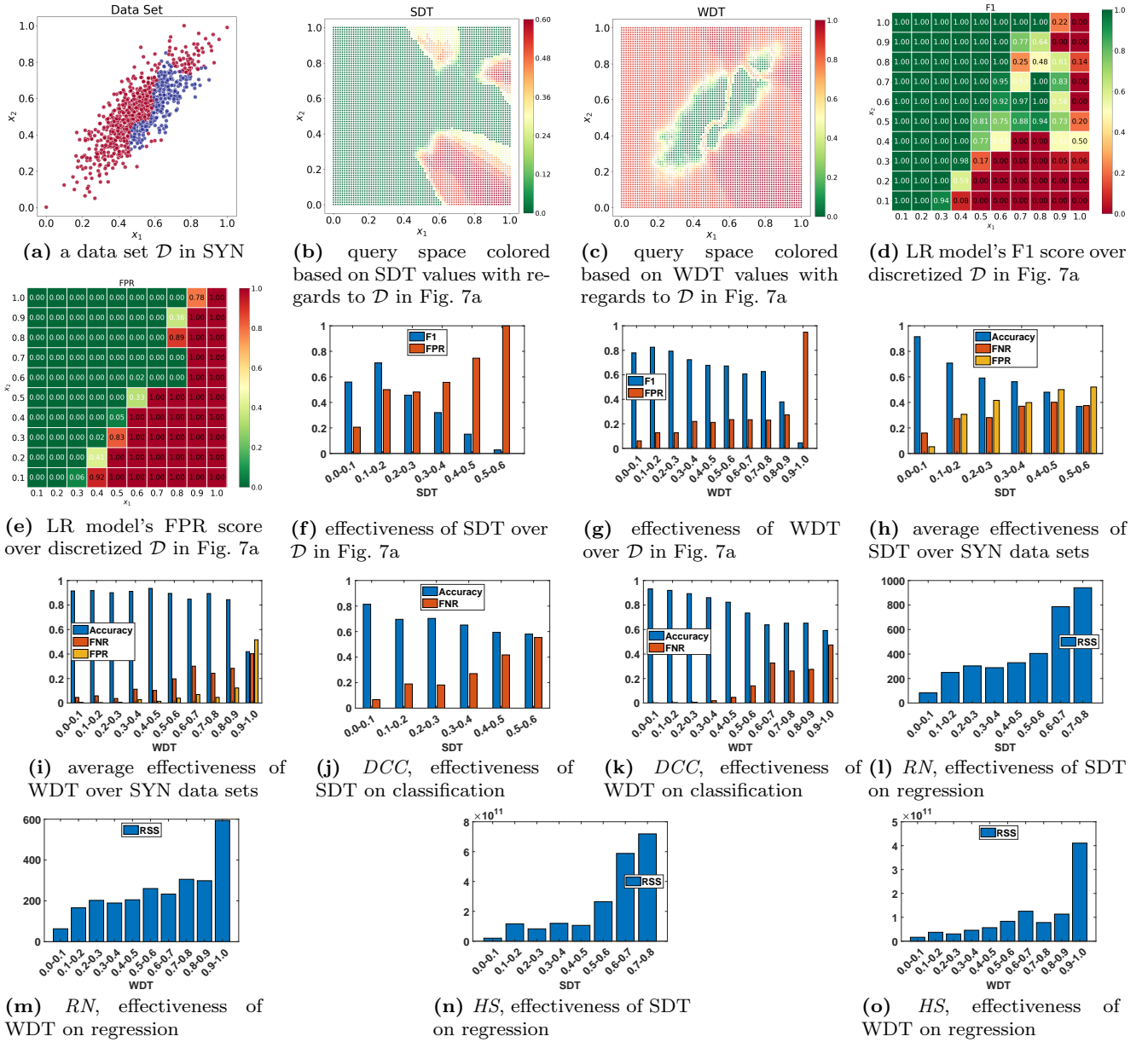


**Fig. 7:** proof of concept results: consistent correlation between distrust values and ML performance metrics.

uniform query space in a  $10 \times 10$  grid and we evaluate the model for each cell to see where it falls short (*a.k.a.* model predictions become less reliable) then we create a heatmap on top of the grid based on the values for each cell. Results are provided in Figures 7d and 7e. In a side-by-side comparison between the heatmaps and the colored space based on SDT and WDT (see Figures 7b, 7c, 7d, and 7e), it is easy to see that the model failed in the regions where the distrust measures are producing large values. Finally, we generate the bar graphs with a similar procedure as later discussed in 7.2 and are shown in Figures 7f and 7g. As the distrust value increases, the F1 score of the model drops while the FPR rises meaning that, the model fails for

the regions that are untrustworthy with regard to our distrust measures. In Figure 7f, as SDT increases, the accuracy measures for the model rapidly drop, and for the 0.5-0.6 bucket, F1 is near zero. This confirms that while WDT is a weaker warning, SDT should be viewed as a red flag.

**Validation on Classification:** Having provided the visual validation results, we next validate our distrust measures on classification tasks. In this regard, using *SYN* data set, we first computed the distrust measures for all the query points in the uniform sample and bucketized the points with respect to their distrust values in ranges of length 0.1. We repeated this for both SDT and WDT measures. Next, using a classification model

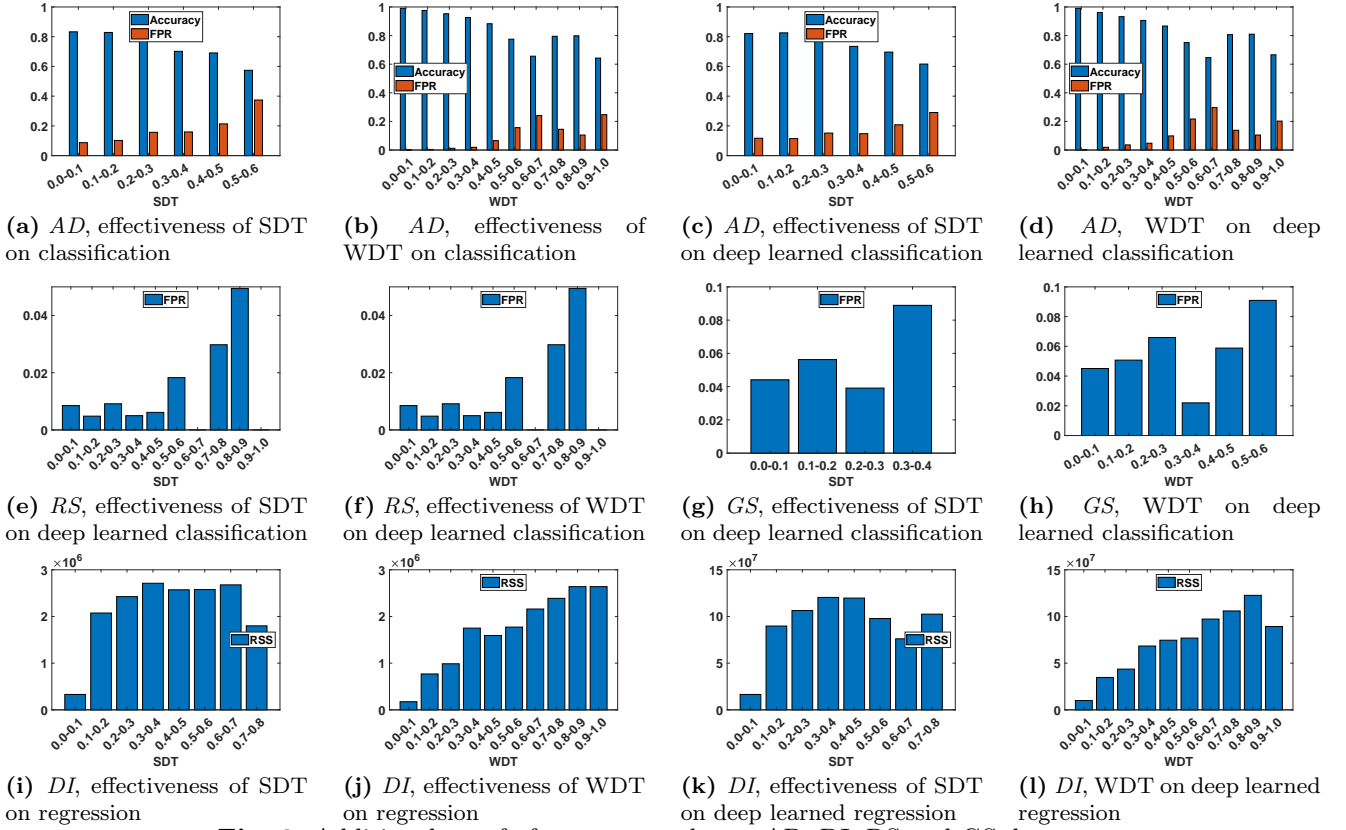


**Fig. 8:** Additional proof of concept results on *AD*, *DI*, *RS* and *GS* datasets.

that we trained on the (training) data set, we predict the target variable for the points in each range of distrust measure. The values corresponding to accuracy/error measures of the classifier over each bucket of distrust values are provided in Figure 7h and 7i for SDT and WDT respectively. As the distrust values increase, the accuracy of the model drops while the FNR and FPR rise, and therefore, the model fails to capture the ground truth for the points that fall into untrustworthy regions in the data set.

To also perform the experiments on a real-world data set, we next used the *DCC* data set with a similar procedure. The results are shown in Figure 7j and 7k and they follow the same course as the previous experiment.

We repeated the experiments with five classification algorithms including, Logistic Regression (LR), K-Nearest-Neighbor ( $k$ -NN), Neural Networks (NN), Random Forest (RF), and SVM. All the classifiers underwent a hyperparameter tuning procedure to achieve optimal prediction correctness. We confirm that we obtained similar results in all cases and that all models failed to predict satisfactorily for query points that have a high distrust value. Hence, we provide the results for the NN model, the more advanced and powerful model. Depending on the results of the classification, we chose

the most appropriate accuracy/error measures that indicated the behavior of the model. For example, if the results were dominated by TPs and TNs, accuracy is the measure that best describes the model, otherwise, F1 might be a better choice. Depending on the number of FPs and FNs and the balance between them, the same rule applies to FPR and FNR measures.

Finally, to stress test our proposed measures with more complex learning tasks (such as complex classifiers, massive high dimensional data sets based on NLP and vision tasks, sparse data sets, etc.), we extended our experiments to three other classification data sets, *AD*, *RS*, and *GS*. Initially, we repeated the experiments with identical settings as before. For *AD*, the results are shown in Figures 8a and 8b and corroborate our findings. For tuples with high distrust values, models tend to fail more to predict reliably. Next, we repeated the experiments on *AD*, using deep learning. We trained a classification model (with tuned parameters) with two hidden layers of size 64 and 32 units respectively. We also constructed and tuned deep-learning models for *RS*, and *GS* data sets. The results are illustrated in Figures 8c, 8d, 8e, 8f, 8g, and 8h and are compliant with our previous experiments, showing that even with the choice of more complex models that show promising results in the tasks (95% F1 score in the case of

*RS*), they still are less reliable for query points with high distrust values. Models' accuracy in Figures 8e–8h were consistently above 95% in all cases. Therefore, for visual clarity we only included FPR.

**Validation on Regression:** In this experiment, we study the effectiveness of our distrust measures in the regression tasks. Accordingly, we used *RN* and *HS* data sets and computed SDT and WDT distrust values for all the query points in the uniform sample. Thereafter, we repeated the bucketization process as we did in the last experiment, and having trained a regression model over the data set, we evaluate the model's prediction over the tuples from each bucket. The results are presented in Figures 7l, 7m, 7n and 7o. As the distrust value increases, the RSS of the regression model follows the same trend denoting that the model fails to perform for tuples with a high distrust value. We repeated the experiments with 3 different regression algorithms including ElasticNet, DT, and *k*-NN, all three with tuned hyper-parameters. Regardless of the regression model, the outcome was similar and therefore we only report the results for the *k*-NN regressor.

Finally, using the *DI* data set, we repeated the experiments with identical settings as before. The results are brought in Figures 8i, 8j verifying our findings. For tuples with high distrust values, models fail more frequently. Next, we repeated the experiments on *DI*, using a Deep Learning regression model with tuned parameters. We constructed a regression model with four hidden layers of size 128, 64, 32, and 16 respectively. The results are shown in Figures 8k, 8l and are consistent with the previous experiments, verifying that even more complex models fail for query points with high distrust values.

**Summary of Proof of Concept:** In short, experiments consistently demonstrate that as the distrust values grow, the ML models become less reliable in capturing the truth for the corresponding regions. Consequently, when distrust values for a query point in a data set are high, one should discard or at least not rely on the outcome of the model constructed on it for critical decisions.

### 7.3 Comparison with the Existing Work

In this section, we thoroughly evaluate the distrust measures in the context of the existing approaches discussed in §2, demonstrate why the existing approaches fail, and how distrust measures are superior in capturing the unreliability of individual predictions.

Consider data set  $\mathcal{D}$  as shown in Figure 9a created with three Gaussian distributions representing classes *red*, *blue*, *orange*. An arbitrary classification model (e.g.

Gaussian Naive Bayes classifier) as the base classifier is trained on  $\mathcal{D}$  and the predicted labels are depicted in Figure 9b. Finally, Figures 9i and 9j show the corresponding SDT and WDT values for data set  $\mathcal{D}$ .

Through the rest of this section, we use the data set  $\mathcal{D}$  and the classifier described above to evaluate the existing approaches for reliability of individual predictions.

#### 7.3.1 Conformal Prediction

We start by employing the conformal prediction (CP) framework with confidence level  $\alpha$  of 0.2, 0.1, and 0.05 and softmax score output of the base classifier as the conformity score. Results are shown in Figures 9c, 9d, 9e. As can be seen in Figure 9c, CP is creating empty prediction sets for  $\alpha = 0.2$  for query points around the uncertain areas which are faulty and show that CP is highly dependent on the choice of  $\alpha$ . The null region disappears for larger  $\alpha$  values but ambiguous classification regions arise with several labels included in the prediction sets highlighting the uncertain behavior of the base classifier. By choosing the cumulative softmax conformal score, the empty prediction set problem is resolved however, uncertain regions are emphasized by wider boundaries. Now consider the query point  $q$ ; according to the model prediction,  $q$  belongs to the *orange* class and regardless of the chosen  $\alpha$ , CP confirms that. However, this is only true if the true decision boundary is identical to the one estimated by the base classifier, however, as previously discussed in section 4.1, this may not always be the case. Therefore, although  $q$  is in an uncertain region, CP fails to capture it. Conversely, as can be seen in Figure 9j, the WDT measure can successfully capture the distrust associated with  $q$  as it is an outlier, yet does not belong to an uncertain region.

#### 7.3.2 Prediction Probabilities

In the next experiment, we evaluate the prediction probabilities generated by probabilistic classification models and demonstrate their failure for query points that are not represented by data. To do so, we employ data set  $\mathcal{D}$  and train an arbitrary probabilistic classifier such as Gaussian Naive Bayes on it (remember that we can use any classifier, however, if the model is not intrinsically probabilistic, we need to make sure that the probabilistic outcomes are calibrated). Figures 10a, 10b, and 10c show the prediction probabilities assigned to either of the classes *red*, *blue* and *orange*. As it can be observed, prediction probabilities fail to capture query points that belong to unrepresented regions and assign a negligible

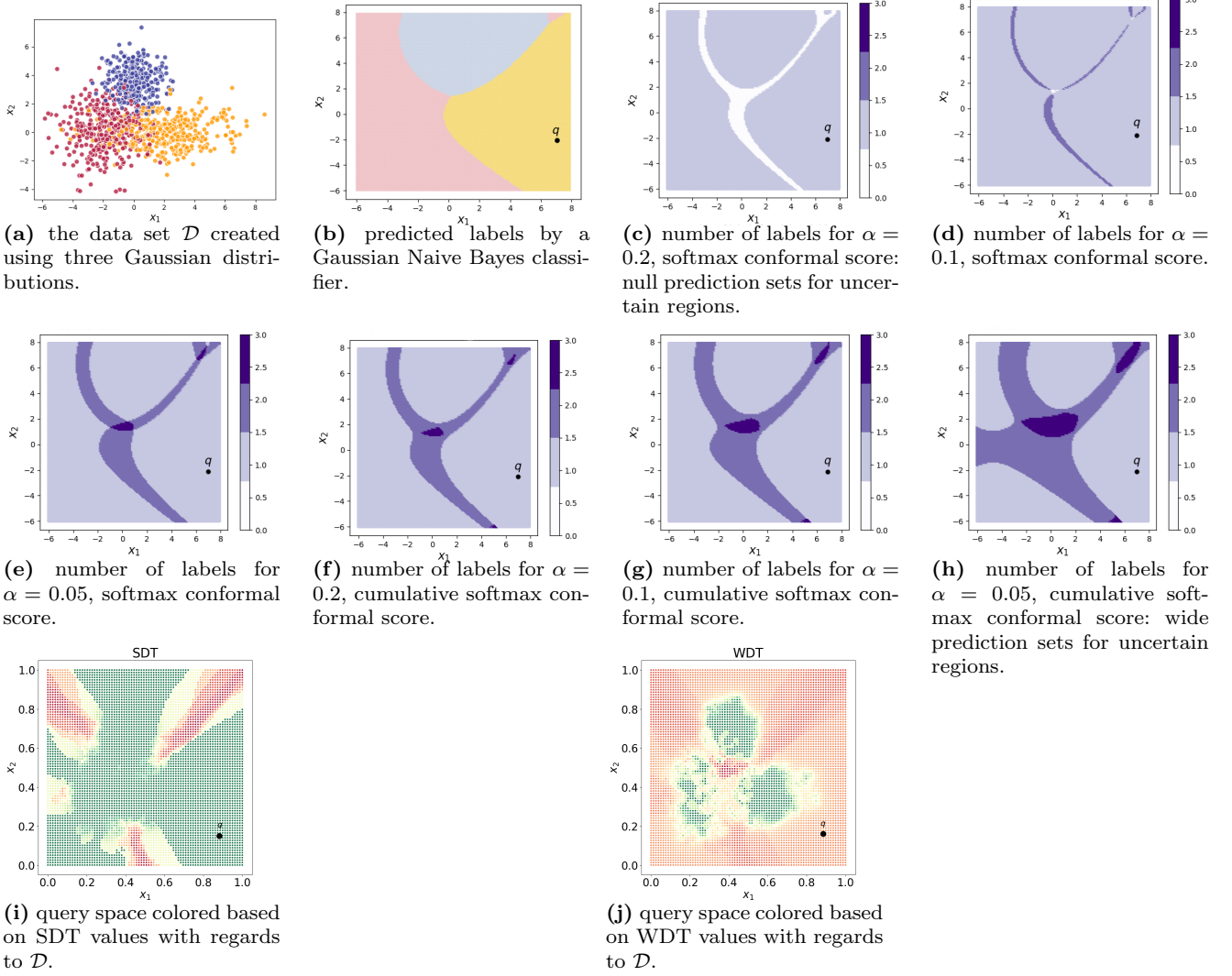


**Fig. 9:** Conformal Prediction fails to detect the prediction unreliability for not well-represented point  $\mathbf{q}$  while WDT correctly captures such unreliability.

chance of belonging to any other class but the one determined by the decision boundary, however, this is only true if the true decision boundary is identical to the one estimated by the base classifier and as previously discussed in §4.1, this may not always be the case if the distribution between training data and production data vary.

### 7.3.3 Data Coverage

Finally, we conduct an experiment to assess the capacity of data coverage techniques to create proper warnings and demonstrate their failure for query points that are in uncertain regions. To this end, using the continuous notion of data coverage [11] and tuned parameters of  $k = 50$  and  $\rho = 0.08$ , we identify the uncovered region on data set  $\mathcal{D}$  as illustrated in Figure 11. The

training data points ( $\mathcal{D}$ ) are highlighted as black dots. The regions highlighted in red and green comprise the uncovered and covered regions respectively. Any query point belonging to the green region is covered and all the query points in the red region are uncovered. While the uncovered region can raise warning signals for the unreliability of underrepresented query points, it fails to capture the unreliability associated with the uncertain regions (regions close to the decision boundary in the case of data set  $\mathcal{D}$ ). Furthermore, even for the query points in underrepresented regions, data coverage creates a binary value that is sensitive to the choice of parameters such as the radius  $\rho$ . This issue gets further highlighted considering the sharp transition from uncovered to covered, specified by the uncovered region's decision boundary. As a result, while two points close to each other, where one is inside and the other



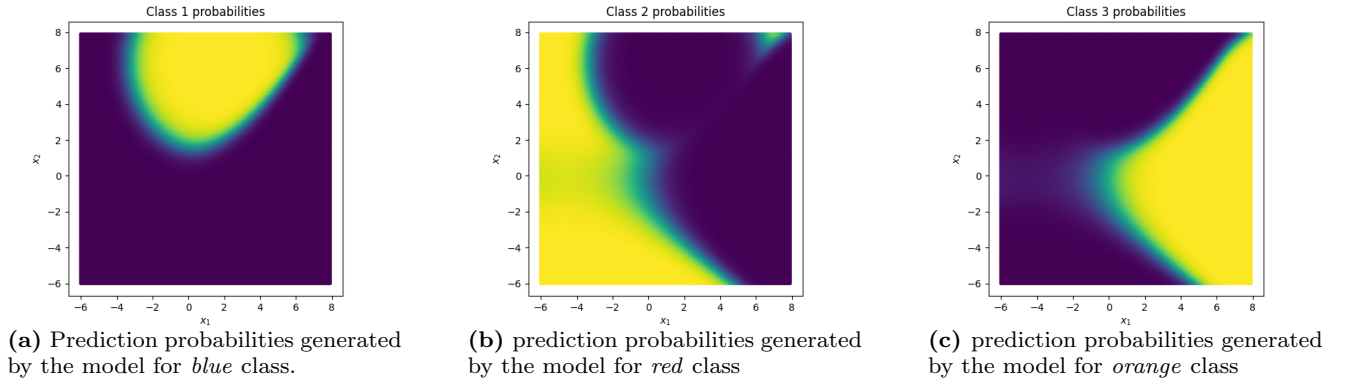


**Fig. 10:** Prediction probabilities of classifiers trained on  $\mathcal{D}$  in Figure 9a fails for query points that are not well-represented.

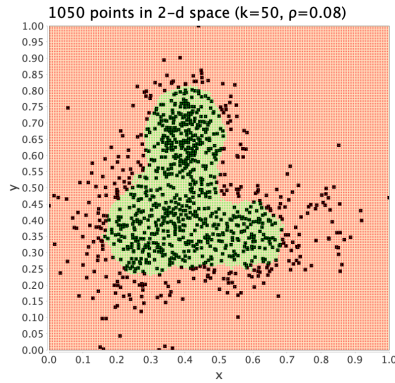


**Fig. 11:** data coverage on data set  $\mathcal{D}$  in Figure 9a fails to capture the unreliability associated with the query points in uncertain regions. The training data ( $\mathcal{D}$ ) are highlighted as black dots. The regions highlighted in red and green comprise the uncovered and covered regions respectively. Any query point belonging to the green (red) region is considered (un)covered.

outside of the decision boundary, are almost equally miss-presented, for one the output signal is covered (no warning at all) while the other is uncovered (maximum warning).

## 7.4 Performance Evaluations

After demonstrating the effectiveness of the distrust measures, we now focus on the performance of our algorithms. In this section, we use the *DCC* and *RN* data sets to evaluate the time efficiency of algorithms. We obtained similar results with almost identical plots for both classification and regression tasks. In the following, we present the results for classification tasks using *DCC* data set with different settings.

### 7.4.1 Query Time

The query time consists of (i) the time to find the  $k$ -vicinity of the query point  $q$  and identifying the tuple in  $k$ -vicinity that has the maximum distance from  $q$ , and (ii) the time to apply binary search on the sorted multi-sets.

**Varying  $n$ :** To study the impact of the number of tuples  $n$  on the performance of the query time, we gradually increase the size of the data set from 50 to 100K. The results are provided in Figure 12a. The total query time is dominated by the first bottleneck, and the time to binary search the lists are negligible compared to it. In our experiments, the query time did not (meaningfully) change as the data set size increased, showing the scalability of our algorithm to the very large settings.

**Varying  $k$ :** Next, we vary the neighborhood size  $k$  from 1 to 50. The results in Figure 12b suggest that the query time is (almost) independent from the  $k$ .

**Varying  $d$ :** We next study the impact of the number of attributes  $d$  by varying it from 2 to 20. The results in Figure 12c verify the scalability of our algorithms with respect to the number of dimensions.

**Varying  $c$ :** In our final experiment, we change  $c$  from 0.05 to 0.25. The results are brought in Figure 12d. Results verify that the query time is independent of the  $c$ .

### 7.4.2 Preprocessing Time

Our preprocessing time consists of two parts. The first is the time to build the  $k$ -NN data structure, identifying the  $k$ -vicinity radius (in Algorithm 1) and computing uncertainty (in Algorithm 2) for each tuple in the data set. The second one is the time to construct the sorted multi-sets of  $k$ -vicinity radii and uncertainty values. We

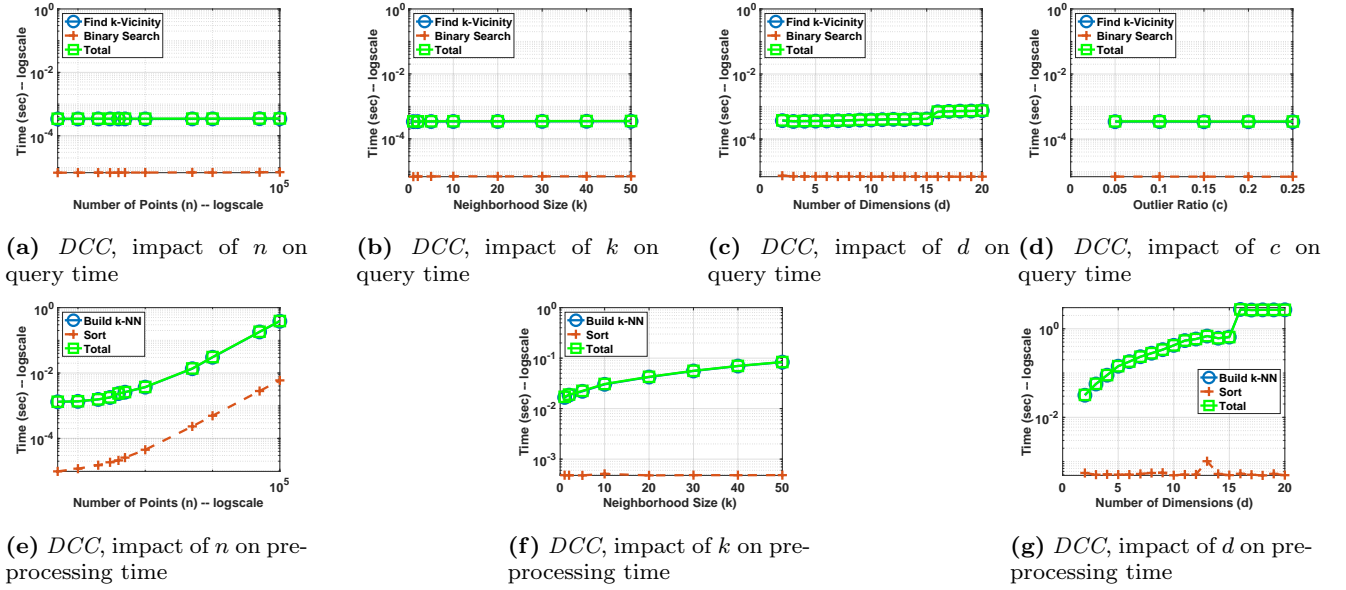


Fig. 12: performance evaluation results

use the exact  $k$ -vicinity radii and entropy values in this experiment.

**Varying  $n$ :** In this experiment, we study the impact of the number of tuples  $n$  in the data set on the pre-processing time by gradually increasing the size of the data set from 50 to 100K. We then measure the time to build the  $k$ -NN data structure and construct the sorted multi-sets. The results are provided in Figure 12e. The total preprocessing time is dominated by the time to build the  $k$ -NN data structure and the time to build the multi-sets is almost negligible compared to it. Nevertheless, the cumulative preprocessing time was small enough that the algorithm could scale to larger settings, finishing in less than a second for  $n=100K$ .

**Varying  $k$ :** To study the impact of neighborhood size  $k$  on the preprocessing time, we vary  $k$  from 1 to 50. The results can be seen in Figure 12f. Similarly, the total preprocessing time in this experiment is also dominated by the time to build the  $k$ -NN data structure and the algorithm was efficient in all settings, finishing in less than a fraction of a second for  $k=50$ .

**Varying  $d$ :** To study the impact of the number of attributes  $d$  of the data set on the preprocessing time, we gradually change  $d$  from 2 to 20. The results are brought in Figure 12g. Like the previous settings, the total preprocessing time is dominated by the time to build the  $k$ -NN data structure and the algorithm linearly scales to larger settings, finishing in less than 3 seconds for  $d=20$ .

## 7.5 Impact of Distance Measures on The Distrust Values

In this experiment, we study the effect of the distance metric chosen to determine the neighborhood of a data point (in the  $k$ -NN component) on the distrust values. To do so, we employ data set  $\mathcal{D}$  (Figure 7a) and calculate the distrust values for the entire query space with respect to six distance measures of *braycurtis*, *canberra*, *chebyshev*, *cityblock*, *manhattan* and *euclidean*. Although the distance metric is expected as an input in our implementation, however, the results as depicted in Figures 13, show general consistency across both measures.

### 7.5.1 Training Regression Models for No Data Access

As our final experiment, we study the efficiency of the training process for building the regression models to estimate the values of  $k$ -vicinity radius and entropy. As explained in § 5.3, we apply exponential sampling to generate the right amount of data such that the trained models satisfy the user-specified error. As a heuristic, we generate a fraction of samples uniformly and the others from the underlying distribution of the training data using GAN methods or Gaussian copula distribution functions [63]. Figure 14 illustrates the monotonic drop in the error of both regression models trained to predict the entropy and  $k$ -vicinity radii of query points (as discussed in section 5.3), as the number of synthetic i.i.d samples increases. Since both entropy and  $k$ -vicinity radii values are in the range of  $[0,1]$ , select-



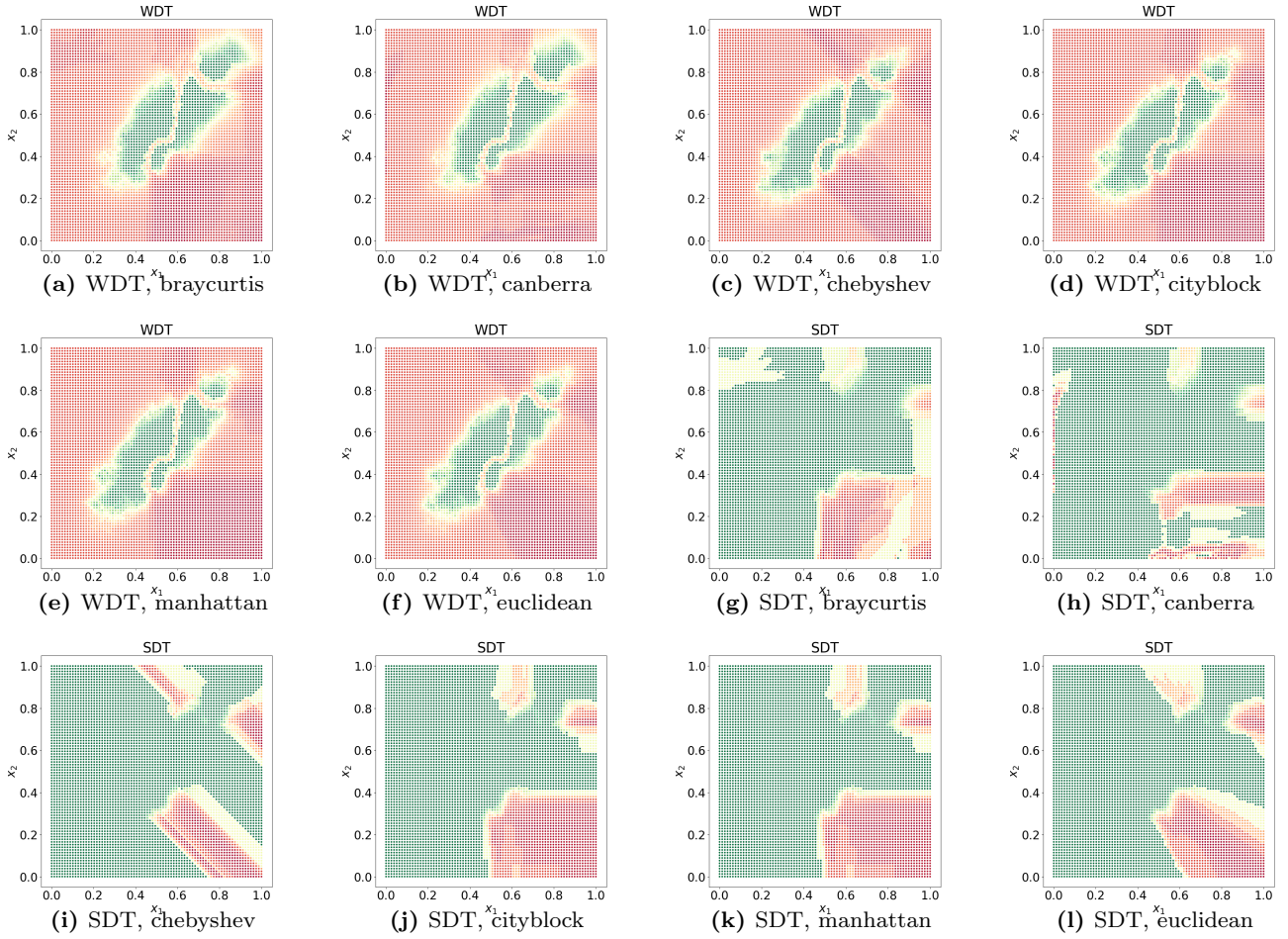


**Fig. 13:** query space colored based on WDT and SDT values with regards to  $\mathcal{D}$  in Fig. 7a subject to different distance metrics.

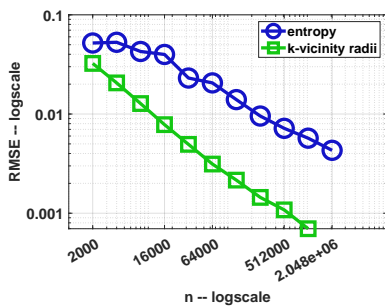


**Fig. 14:** Effectiveness of Exponential Search in reducing the error of learning distrust parameters

ing a sufficiently small (RMSE) error threshold (e.g.  $10^{-3}$  or 0.01% average difference between the actual and predicted values) guarantees not going overboard with generating too many samples (affecting preprocessing time) while achieving good prediction accuracy.

## 8 Conclusion

Towards addressing the need for trustworthy AI, in this paper, we proposed distrust measures as the warning signals that limit datasets' scope of use for predicting future query points. These measures are valuable alongside other techniques for trustworthy AI. We proposed novel ideas for the effective implementation of distrust measures and designed efficient algorithms that scale to very large, high-dimensional data. Our comprehensive experiments on real-world and synthetic data sets validated our proposal and verified the scalability of our algorithms with sub-second run times.

## References

1. Abdar, M., Pourpanah, F., Hussain, S., Rezazadegan, D., Liu, L., Ghavamzadeh, M., Fieguth, P., Cao, X., Khosravi, A., Acharya, U.R., Makarevich, V., Nahavandi, S.: A review of uncertainty quantification in deep learning:

- Techniques, applications and challenges. *Information Fusion* **76**, 243–297 (2021). DOI <https://doi.org/10.1016/j.inffus.2021.05.008>. URL <https://www.sciencedirect.com/science/article/pii/S1566253521001081>
2. Abedjan, Z., Golab, L., Naumann, F., Papenbrock, T.: Data profiling. *Synthesis Lectures on Data Management* **10**(4), 1–154 (2018)
  3. Accinelli, C., Catania, B., Guerrini, G., Minisi, S.: The impact of rewriting on coverage constraint satisfaction. In: *EDBT/ICDT Workshops* (2021)
  4. Accinelli, C., Minisi, S., Catania, B.: Coverage-based rewriting for data preparation. In: *EDBT/ICDT Workshops* (2020)
  5. Agarwal, P.K., De Berg, M., Matousek, J., Schwarzkopf, O.: Constructing levels in arrangements and higher order voronoi diagrams. *SIAM journal on computing* **27**(3), 654–667 (1998)
  6. Agrawal, S.: *Diamonds* (2017). URL <https://www.kaggle.com/datasets/shivam2503/diamonds>
  7. Angelopoulos, A.N., Bates, S.: A gentle introduction to conformal prediction and distribution-free uncertainty quantification. *arXiv preprint arXiv:2107.07511* (2021)
  8. Asudeh, A., Jagadish, H., Stoyanovich, J., Das, G.: Designing fair ranking schemes. In: *SIGMOD*, pp. 1259–1276 (2019)
  9. Asudeh, A., Jagadish, H.V.: Fairly evaluating and scoring items in a data set. *PVLDB* **13**(12), 3445–3448 (2020)
  10. Asudeh, A., Jin, Z., Jagadish, H.: Assessing and remedying coverage for a given dataset. In: *2019 IEEE 35th International Conference on Data Engineering (ICDE)*, pp. 554–565. IEEE (2019)
  11. Asudeh, A., Shahbazi, N., Jin, Z., Jagadish, H.: Identifying insufficient data coverage for ordinal continuous-valued attributes. In: *Proceedings of the 2021 International Conference on Management of Data*, pp. 129–141 (2021)
  12. Barocas, S., Selbst, A.D.: Big data’s disparate impact. *Calif. L. Rev.* **104**, 671 (2016)
  13. Blundell, C., Cornebise, J., Kavukcuoglu, K., Wierstra, D.: Weight uncertainty in neural network. In: F. Bach, D. Blei (eds.) *Proceedings of the 32nd International Conference on Machine Learning, Proceedings of Machine Learning Research*, vol. 37, pp. 1613–1622. PMLR, Lille, France (2015). URL <https://proceedings.mlr.press/v37/blundell115.html>
  14. Bohler, C., Cheilaris, P., Klein, R., Liu, C.H., Papadopoulos, E., Zavershynskiy, M.: On the complexity of higher order abstract voronoi diagrams. In: *International Colloquium on Automata, Languages, and Programming*, pp. 208–219. Springer (2013)
  15. Breiman, L., Friedman, J.H., Olshen, R.A., Stone, C.J.: *Classification and regression trees*. Routledge (2017)
  16. Breunig, M.M., Kriegel, H.P., Ng, R.T., Sander, J.: Lof: identifying density-based local outliers. In: *Proceedings of the 2000 ACM SIGMOD international conference on Management of data*, pp. 93–104 (2000)
  17. Brier, G.W., et al.: Verification of forecasts expressed in terms of probability. *Monthly weather review* **78**(1), 1–3 (1950)
  18. Carlini, N., Erlingsson, U., Papernot, N.: Distribution density, tails, and outliers in machine learning: Metrics and applications. *arXiv preprint arXiv:1910.13427* (2019)
  19. Chandola, V., Banerjee, A., Kumar, V.: Anomaly detection: A survey. *ACM computing surveys (CSUR)* **41**(3), 1–58 (2009)
  20. Chatfield, C.: Prediction intervals. *Journal of Business and Economic Statistics* **11**, 121–135 (1993)
  21. Chazelle, B., Edelsbrunner, H.: An improved algorithm for constructing kth-order voronoi diagrams. *IEEE Transactions on Computers* **100**(11), 1349–1354 (1987)
  22. Dustin, J.: Amazon scraps secret ai recruiting tool that showed bias against women. San Fransico, CA: Reuters. Retrieved on October 9, 2018 (2018)
  23. Dong, X.L., Gabrilovich, E., Murphy, K., Dang, V., Horn, W., Lugaresi, C., Sun, S., Zhang, W.: Knowledge-based trust: Estimating the trustworthiness of web sources. *arXiv preprint arXiv:1502.03519* (2015)
  24. Dressel, J., Farid, H.: The accuracy, fairness, and limits of predicting recidivism. *Science advances* **4**(1), eaao5580 (2018)
  25. Edelsbrunner, H., Seidel, R.: Voronoi diagrams and arrangements. *Discrete & Computational Geometry* **1**(1), 25–44 (1986)
  26. Ester, M., Kriegel, H.P., Sander, J., Xu, X., et al.: A density-based algorithm for discovering clusters in large spatial databases with noise. In: *kdd*, vol. 96, pp. 226–231 (1996)
  27. Fariha, A., Tiwari, A., Radhakrishna, A., Gulwani, S., Meliou, A.: Conformance constraint discovery: Measuring trust in data-driven systems. In: *Proceedings of the 2021 International Conference on Management of Data, SIGMOD/PODS ’21*, p. 499–512. Association for Computing Machinery, New York, NY, USA (2021). DOI 10.1145/3448016.3452795. URL <https://doi.org/10.1145/3448016.3452795>
  28. Fernandez, M.: Study finds disparities in mortgages by race. *New York Times* **15** (2007)
  29. Flores, A.W., Bechtel, K., Lowenkamp, C.T.: False positives, false negatives, and false analyses: A rejoinder to machine bias: There’s software used across the country to predict future criminals. and it’s biased against blacks. *Fed. Probation* **80**, 38 (2016)
  30. Gebel, M.: *Multivariate calibration of classifier scores into the probability space*. Ph.D. thesis, Citeseer (2009)
  31. Gebru, T., Morgenstern, J., Vecchione, B., Vaughan, J.W., Wallach, H., Daumé III, H., Crawford, K.: *Datasheets for datasets*. *arXiv preprint arXiv:1803.09010* (2018)
  32. Goel, S., Rao, J.M., Shroff, R., et al.: Precinct or prejudice? understanding racial disparities in new york city’s stop-and-frisk policy. *The Annals of Applied Statistics* **10**(1), 365–394 (2016)
  33. Gunning, D., Aha, D.: Darpa’s explainable artificial intelligence (xai) program. *AI Magazine* **40**(2), 44–58 (2019)
  34. Guyon, I., Gunn, S., Ben-Hur, A., Dror, G.: Result analysis of the nips 2003 feature selection challenge. *Advances in neural information processing systems* **17** (2004)
  35. Harlfoxem: House sales in king county, usa (2016). URL <https://www.kaggle.com/harlfoxem/housesalesprediction/>
  36. Harradon, M., Druce, J., Ruttenberg, B.: Causal learning and explanation of deep neural networks via autoencoded activations. *arXiv preprint arXiv:1802.00541* (2018)
  37. Hautamaki, V., Karkkainen, I., Franti, P.: Outlier detection using k-nearest neighbour graph. In: *Proceedings of the 17th International Conference on Pattern Recognition, 2004. ICPR 2004.*, vol. 3, pp. 430–433 Vol.3 (2004). DOI 10.1109/ICPR.2004.1334558
  38. Jayasinghe, U., Otebolaku, A., Um, T.W., Lee, G.M.: Data centric trust evaluation and prediction framework for iot. In: *2017 ITU Kaleidoscope: Challenges for a Data-Driven Society (ITU K)*, pp. 1–7. IEEE (2017)
  39. Jin, Z., Xu, M., Sun, C., Asudeh, A., Jagadish, H.: Mithracoverage: A system for investigating population

- bias for intersectional fairness. In: Proceedings of the 2020 ACM SIGMOD International Conference on Management of Data, pp. 2721–2724 (2020)
40. Kakade, S.M.: On the sample complexity of reinforcement learning. University of London, University College London (United Kingdom) (2003)
  41. Kaul, M., Yang, B., Jensen, C.S.: Building accurate 3d spatial networks to enable next generation intelligent transportation systems. In: 2013 IEEE 14th International Conference on Mobile Data Management, vol. 1, pp. 137–146. IEEE (2013)
  42. Kentour, M., Lu, J.: Analysis of trustworthiness in machine learning and deep learning. InfoComp (2021)
  43. Khosravi, A., Nahavandi, S., Creighton, D., Atiya, A.F.: Lower upper bound estimation method for construction of neural network-based prediction intervals. IEEE transactions on neural networks **22**(3), 337–346 (2010)
  44. Khosravi, A., Nahavandi, S., Creighton, D., Atiya, A.F.: Comprehensive review of neural network-based prediction intervals and new advances. IEEE Transactions on neural networks **22**(9), 1341–1356 (2011)
  45. Kohavi, R., et al.: Scaling up the accuracy of naive-bayes classifiers: A decision-tree hybrid. In: Kdd, vol. 96, pp. 202–207 (1996)
  46. Kuhlman, C., Rundensteiner, E.: Rank aggregation algorithms for fair consensus. PVLDB **13**(12), 2706–2719 (2020)
  47. Kulynych, B., Yang, Y.Y., Yu, Y., Błasiok, J., Nakkiran, P.: What you see is what you get: Distributional generalization for algorithm design in deep learning. arXiv preprint arXiv:2204.03230 (2022)
  48. LeCun, Y., Cortes, C.: MNIST handwritten digit database (2010). URL <http://yann.lecun.com/exdb/mnist/>
  49. Lee, D.T.: On k-nearest neighbor voronoi diagrams in the plane. IEEE transactions on computers **100**(6), 478–487 (1982)
  50. Lin, Y., Guan, Y., Asudeh, A., Jagadish, H.: Identifying insufficient data coverage in databases with multiple relations. Proceedings of the VLDB Endowment **13**(12), 2229–2242 (2020)
  51. Liu, F.T., Ting, K.M., Zhou, Z.H.: Isolation forest. In: 2008 eighth IEEE international conference on data mining, pp. 413–422. IEEE (2008)
  52. Liu, H., Wang, Y., Fan, W., Liu, X., Li, Y., Jain, S., Jain, A.K., Tang, J.: Trustworthy ai: A computational perspective. arXiv preprint arXiv:2107.06641 (2021)
  53. Lundberg, S.M., Lee, S.I.: A unified approach to interpreting model predictions. Advances in neural information processing systems **30** (2017)
  54. McCallum, A.: real-sim data set. URL <https://www.csie.ntu.edu.tw/~cjlin/libsvmtools/datasets/binary.html#real-sim>
  55. McCallum, A.: Sraa data set. URL <https://people.cs.umass.edu/~mccallum/data.html>
  56. Molnar, C.: Interpretable machine learning. Lulu. com (2020)
  57. Moskovitch, Y., Jagadish, H.: Countata: dataset labeling using pattern counts. Proceedings of the VLDB Endowment **13**(12), 2829–2832 (2020)
  58. Moskovitch, Y., Jagadish, H.: Reliability at multiple stages in a data analysis pipeline. Communications of the ACM **65**(11), 118–128 (2022)
  59. Nargesian, F., Asudeh, A., Jagadish, H.: Tailoring data source distributions for fairness-aware data integration. Proceedings of the VLDB Endowment **14**(11) (2021)
  60. Ng, A.: Mlops: From model-centric to data-centric ai (2021)
  61. Niculescu-Mizil, A., Caruana, R.: Predicting good probabilities with supervised learning. In: Proceedings of the 22nd international conference on Machine learning, pp. 625–632 (2005)
  62. Pakdaman Naeini, M., Cooper, G., Hauskrecht, M.: Obtaining well calibrated probabilities using bayesian binning. Proceedings of the AAAI Conference on Artificial Intelligence **29**(1) (2015). URL <https://ojs.aaai.org/index.php/AAAI/article/view/9602>
  63. Patki, N., Wedge, R., Veeramachaneni, K.: The synthetic data vault. In: 2016 IEEE International Conference on Data Science and Advanced Analytics (DSAA), pp. 399–410 (2016). DOI 10.1109/DSAA.2016.49
  64. Pearce, T., Brintrup, A., Zaki, M., Neely, A.: High-quality prediction intervals for deep learning: A distribution-free, ensembled approach. In: International conference on machine learning, pp. 4075–4084. PMLR (2018)
  65. Platt, J., et al.: Probabilistic outputs for support vector machines and comparisons to regularized likelihood methods. Advances in large margin classifiers **10**(3), 61–74 (1999)
  66. Ramaswamy, S., Rastogi, R., Shim, K.: Efficient algorithms for mining outliers from large data sets. SIGMOD Rec. **29**(2), 427–438 (2000). DOI 10.1145/335191.335437. URL <https://doi.org/10.1145/335191.335437>
  67. Ribeiro, M.T., Singh, S., Guestrin, C.: "why should i trust you?" explaining the predictions of any classifier. In: Proceedings of the 22nd ACM SIGKDD international conference on knowledge discovery and data mining, pp. 1135–1144 (2016)
  68. Salimi, B., Howe, B., Suciu, D.: Database repair meets algorithmic fairness. ACM SIGMOD Record **49**(1), 34–41 (2020)
  69. Salimi, B., Rodriguez, L., Howe, B., Suciu, D.: Interventional fairness: Causal database repair for algorithmic fairness. In: SIGMOD, pp. 793–810 (2019)
  70. Shafer, G., Vovk, V.: A tutorial on conformal prediction. Journal of Machine Learning Research **9**(3) (2008)
  71. Shah, N.B., Lipton, Z.: Sigmod 2020 tutorial on fairness and bias in peer review and other sociotechnical intelligent systems. In: SIGMOD, pp. 2637–2640 (2020)
  72. Shannon, C.E.: A mathematical theory of communication. The Bell system technical journal **27**(3), 379–423 (1948)
  73. Sindhvani, V., Keerthi, S.S.: Large scale semi-supervised linear svms. In: Proceedings of the 29th annual international ACM SIGIR conference on Research and development in information retrieval, pp. 477–484 (2006)
  74. Singh, R., Vatsa, M., Ratha, N.: Trustworthy ai. In: 8th ACM IKDD CODS and 26th COMAD, pp. 449–453 (2021)
  75. Stoyanovich, J., Howe, B.: Nutritional labels for data and models. IEEE Data Eng. Bull. **42**(3), 13–23 (2019)
  76. Stoyanovich, J., Howe, B., Jagadish, H.: Responsible data management. PVLDB **13**(12), 3474–3488 (2020)
  77. Suguna, N., Thanushkodi, K.: An improved k-nearest neighbor classification using genetic algorithm. International Journal of Computer Science Issues **7**(2), 18–21 (2010)
  78. Sun, C., Asudeh, A., Jagadish, H., Howe, B., Stoyanovich, J.: Mithralabel: Flexible dataset nutritional labels for responsible data science. In: Proceedings of the 28th ACM International Conference on Information and Knowledge Management, pp. 2893–2896 (2019)

79. Sweeney, L.: Discrimination in online ad delivery. *Queue* **11**(3), 10–29 (2013)
80. Tae, K.H., Whang, S.E.: Slice tuner: A selective data acquisition framework for accurate and fair machine learning models. In: *Proceedings of the 2021 International Conference on Management of Data*, pp. 1771–1783 (2021)
81. Vapnik, V.N.: An overview of statistical learning theory. *IEEE transactions on neural networks* **10**(5), 988–999 (1999)
82. Venkatasubramanian, S.: Algorithmic fairness: Measures, methods and representations. In: *PODS*, pp. 481–481 (2019)
83. Wing, J.M.: Trustworthy ai. *CACM* **64**(10), 64–71 (2021)
84. Wu, Y., Ianakiev, K., Govindaraju, V.: Improved k-nearest neighbor classification. *Pattern recognition* **35**(10), 2311–2318 (2002)
85. Xu, Z., Kakde, D., Chaudhuri, A.: Automatic hyperparameter tuning method for local outlier factor, with applications to anomaly detection. In: *2019 IEEE International Conference on Big Data (Big Data)*, pp. 4201–4207. IEEE Computer Society, Los Alamitos, CA, USA (2019). DOI 10.1109/BigData47090.2019.9006151. URL <https://doi.ieeecomputersociety.org/10.1109/BigData47090.2019.9006151>
86. Yeh, I.C., hui Lien, C.: The comparisons of data mining techniques for the predictive accuracy of probability of default of credit card clients. *Expert Systems with Applications* **36**(2, Part 1), 2473–2480 (2009). DOI <https://doi.org/10.1016/j.eswa.2007.12.020>. URL <https://www.sciencedirect.com/science/article/pii/S0957417407006719>
87. Zadrozny, B., Elkan, C.: Obtaining calibrated probability estimates from decision trees and naive bayesian classifiers. In: *Icml*, vol. 1, pp. 609–616. Citeseer (2001)
88. Zadrozny, B., Elkan, C.: Transforming classifier scores into accurate multiclass probability estimates. In: *Proceedings of the eighth ACM SIGKDD international conference on Knowledge discovery and data mining*, pp. 694–699 (2002)
89. Zhang, H., Chu, X., Asudeh, A., Navathe, S.B.: Omni-fair: A declarative system for model-agnostic group fairness in machine learning. In: *Proceedings of the 2021 International Conference on Management of Data*, pp. 2076–2088 (2021)
90. Zhang, H., Shahbazi, N., Chu, X., Asudeh, A.: Fairrover: explorative model building for fair and responsible machine learning. In: *Proceedings of the Fifth Workshop on Data Management for End-To-End Machine Learning*, pp. 1–10 (2021)
91. Zhang, Y., Liao, Q.V., Bellamy, R.K.E.: Effect of confidence and explanation on accuracy and trust calibration in ai-assisted decision making. In: *Proceedings of the 2020 Conference on Fairness, Accountability, and Transparency, FAT\* '20*, p. 295–305. Association for Computing Machinery, New York, NY, USA (2020). DOI 10.1145/3351095.3372852. URL <https://doi.org/10.1145/3351095.3372852>